

FUNDAMENTAL METALLURGY OF NIOBIUM IN STEEL

Anthony J. DeArdo\*, J. Malcolm Gray\*\*, and Lutz Meyer\*\*\*

\*University of Pittsburgh  
848 Benedum Hall  
Pittsburgh, Pennsylvania 15261 U.S.A.

\*\*Microalloying International  
7670 Woodway - Suite 360  
Houston, Texas 77063 U.S.A.

\*\*\*Thyssen Aktiengesellschaft  
Duisburg-Hamborn, West Germany

Abstract

In the early 1960's, the forerunners of the current microalloyed steels were being studied and fairly well understood, (1-4) and the first conference devoted to these materials was held in Harrogate, England, in 1963 (5). The present paper reviews some of the metallurgical developments which have taken place since then in the alloy design, processing and application of these steels. Particular emphasis has been placed on the basic metallurgical principles which apply to these steels, for it is the application of these principles which allows the composition - processing - microstructure - mechanical property relationships to be rationalized and exploited. The application of basic metallurgical principles has resulted in a predictive capability which has led to alterations in composition and processing for the purpose of producing steels with superior mechanical properties and improved overall performance.

## Introduction

Within the last few decades, the construction, energy and transportation industries have created a demand for economical, high-tonnage steels with continually improved mechanical properties. Candidate steels were expected to be stronger, tougher, more formable, more weldable, while not being appreciably more expensive than the C-Mn steels they were to supercede. The world-wide steel industry met this demand with the development of a complete family of high-strength, low-alloy steels (HSLA) to be used in the hot-rolled, cold-rolled or heat-treated condition.

The multitude of alloying concepts and processing methods documented in the literature for each application, which cannot be described here in detail, is impressive proof of the adaptability and versatility of steel. The different applications and technology of production of niobium-containing steels are described elsewhere in this volume; thus the present paper will merely review the physical metallurgical principles in widespread use. The paper confines discussion to HSLA (microalloyed) steels and does not attempt to cover usage of niobium as a carbide stabilizer in stainless or other highly alloyed steels since these aspects are discussed in context in the relevant papers in this volume.

A microalloying addition to steels is generally regarded as being less than 0.1 percent and usually refers to deliberate additions of niobium, vanadium or titanium to mild steel compositions. The steels may be fully or partially deoxidized depending on the application and thus they represent relatively simple yet dramatic extensions of the mild steels that they replace. Carbon contents vary widely, usually in the range 0.02 to 0.25 percent, although there are notable exceptions in reinforcing bar (up to 0.45% C) and rail steel (up to 0.55% C).

The general trend in structural steels has been to decrease the carbon content and increase the microalloying level in order to obtain high strengths while maintaining good toughness and weldability. Manganese contents range from 0.10 to 0.2 percent in hot-rolled and cold-rolled sheet steels to as high as 2.0 percent or greater in thick plates.

Some elements such as Cu, Ni, Cr and Mo may be present at residual levels or as a result of deliberate additions intended to control austenite decomposition and recrystallization kinetics and to optimize solution and precipitation characteristics of microalloy carbonitrides. Aluminum, boron, oxygen, sulfur and nitrogen have important effects on microalloy steels but are not referred to as microalloying elements even though they may be added deliberately.

The relationships that exist among composition, processing, microstructure and mechanical properties in these microalloyed steels have been extensively studied in the last decade and much of this work has been presented at several excellent conferences (6-13). It has been appreciated for some time that certain metallurgical characteristics are critical to the microstructure/mechanical property relationships exhibited by the steels. These include:

1. Size and shape of grains of the transformation product,
2. Precipitate size and volume fraction,
3. Dislocation density,
4. Non-metallic inclusion volume fraction and shape,
5. Cementite content and distribution, and
6. Texture.

It should be noted at the normal levels of addition (level of solubility in  $\alpha$  and  $\gamma$ ) niobium does not contribute to strength through solid solution hardening.

A fine ferrite grain size results in increased strength, decreased impact transition temperature (FATT) and improved resistance to ductile fracture. The latter two are especially important considerations in thick-gauge material where toughness becomes of critical importance. A low carbon content can have three potential benefits: high toughness (higher ductile fracture energy and lower FATT), improved weldability and more efficient solution and precipitation of microalloy carbonitrides. Precipitation of microalloy carbonitrides in the austenite is important since this can control the recrystallization of deformed austenite, whereas precipitation in ferrite would result in precipitation hardening. A high dislocation density can lead to high strengths and rates of work hardening. Finally, the absence of elongated inclusions reduces the anisotropy in ductile fracture behavior by improving both the long-transverse and short-transverse ductilities. The metallurgical characteristics noted above can result in a hot-rolled steel that is strong, tough, weldable and formable. For cold-rolled steel, processing conditions are chosen either to achieve high strength or desirable planar anisotropy for purposes of improving formability, whereas for heat-treated steels, maximum austenite grain refinement resulting from carbonitride distributions is an important objective.

In summary, the last two decades have witnessed the evolution of a complex family of economically viable engineering steels which is based on the concept of choosing the proper combination of composition and thermo-mechanical treatment that will result in a specific, final microstructure, and, hence, excellent final mechanical properties.

#### Benefits of Using Niobium in Microalloyed Steel

The multiplicity of options afforded by microalloyed steels for property manipulation can be traced to two important points.

1. Vanadium, titanium and niobium have limited solubility in austenite.
2. All three elements form nitrides and carbides. The relative stability of these compounds is reflected in their differential effects on metallurgical reactions controlling the properties of microalloyed steel.

Control of the solution and reprecipitation of microalloy carbides and nitrides is the basic building block of HSLA technology. In most steels, niobium is in solution at the slab reheating temperature, but when present in excess it acts to refine the austenite grain size. During rolling, niobium retards the recovery and recrystallization processes which form the basis for thermomechanical treatments, and its effectiveness in small amounts distinguishes it from other microalloying elements. Thermomechanical treatments are critical to most microalloyed steels, since they could not possibly develop their final combinations of mechanical properties from their chemical makeup alone. Thus, niobium is viewed as the key ingredient in many HSLA steels and is regarded as the most effective grain refiner of hot-rolled products.

The effect of the grain refinement and sub-grain refinement on yield strength can be expressed by the familiar Petch relationship, Figure 1 (14, 15) whereas the corresponding improvement in toughness is shown in Figure 2 (16).

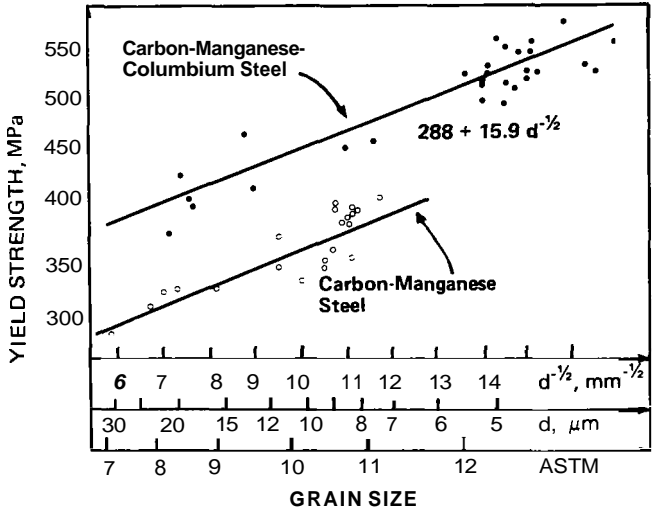


Figure 1 (a) - Experimental Hall-Petch relationships determined by quantitative metallography for carbon-manganese and carbon-manganese-columbium steels. After LeBon and Saint-Martin (14).

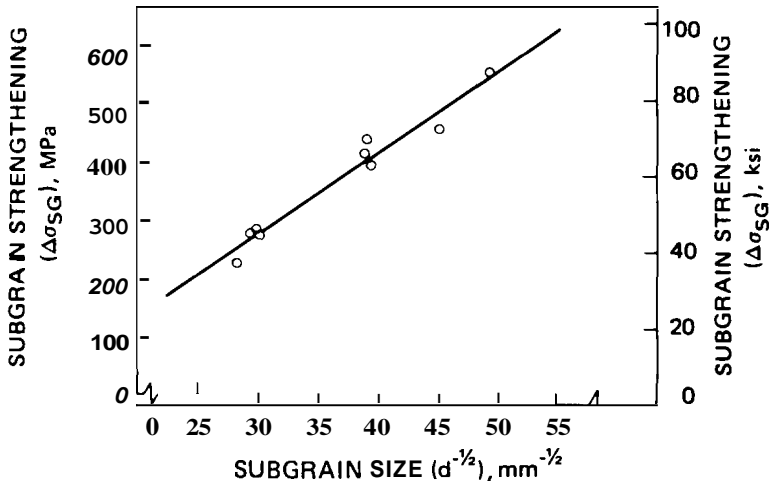


Figure 1 (b) - Hall-Petch Relationship for Subgrains in Controlled Rolled Microalloy Steels. After Mangonon and Heitmann (15).

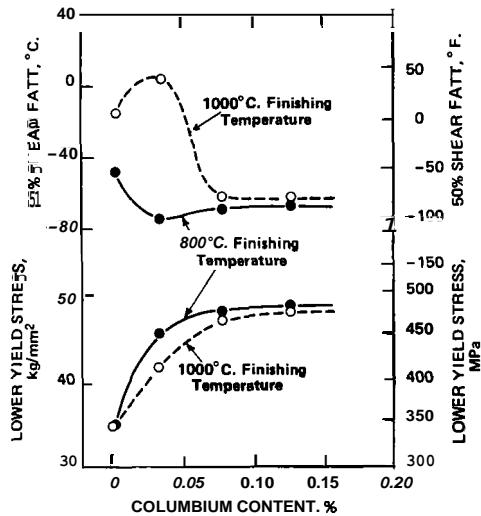


Figure 2 - Effect of columbium on lower yield stress and transverse 50 percent shear fracture-appearance transition temperature (FATT) for 20-mm thick steel with a 0.08 percent carbon, 0.25 percent silicon, and 1.50 percent manganese base composition. The reheating temperature was 1250 C. After Kozasu et al (16).

Niobium remaining in solution after rolling will usually precipitate in ferrite either during or after transformation and will increase strength through classical precipitation hardening mechanisms. However, when cooling rates are rapid or when transformation temperatures are depressed through alloying, precipitation may be suppressed and will only occur during subsequent aging treatments. If reheating is continued into the austenite region, for instance before normalizing or quenching and tempering, niobium is effective in preventing grain growth.

When niobium is present in the correct stoichiometric amounts, the high stability of niobium carbide and nitride in ferrite yield important technological applications in reducing free interstitial contents to very low levels. Significant applications include use in chromium plate steels, "interstitial free" sheet steels and in normalized steels in conjunction with aluminum to prevent strain aging. In this latter case, and other cold-rolled steels, the precipitates may affect the development of the deformation and recrystallization textures which lead to the characteristic anisotropy of sheet steels.

Utilization of the above characteristics of niobium in steel allows steelmakers to produce a wide spectrum of products at relatively low cost and it seems likely that the historical trends of growth in consumption (10% per year) will continue for the foreseeable future.

## Processing of Niobium Steels

During steel manufacture the different products undergo a variety of thermal and mechanical manipulations that affect their final mechanical properties. Metallurgical changes take place during each stage which affect metallurgical responses in subsequent phases as the solutes and carbonitride phases are repeatedly redissolved and precipitated. This sequential processing can give rise to cumulative effects (inheritance or memory-like effects) which are surprisingly complicated for HSLA steels. Furthermore, the magnitude of each metallurgical reaction is affected by the overall constitution of the steels and the alloying concepts being used. It seems reasonable to predict that present trends toward direct rolling will affect the relative magnitude of the "inheritance" factors.

The processing steps for representative HSLA products are shown diagrammatically in Figure 3 and their thermometallurgical significance is briefly described below.

### Casting

Solidification microstructures have been inadequately studied even though they are relevant to continuous casting behavior. A few metallographic results have been presented showing precipitate distributions in cast low carbon Mn-Mo-Nb steel (17, 18) but more extensive correlation is required between grain structure, precipitation phenomena and the overall constitution of the steel.

There are indications that niobium acts like titanium (19) to refine columnar dendritic structures (20) and to modify weld metal microstructures (21-23). Present investigations are focused on the peritectic reaction in Fe-C-Mn-Nb alloys and its influence on ductility of cast structures.

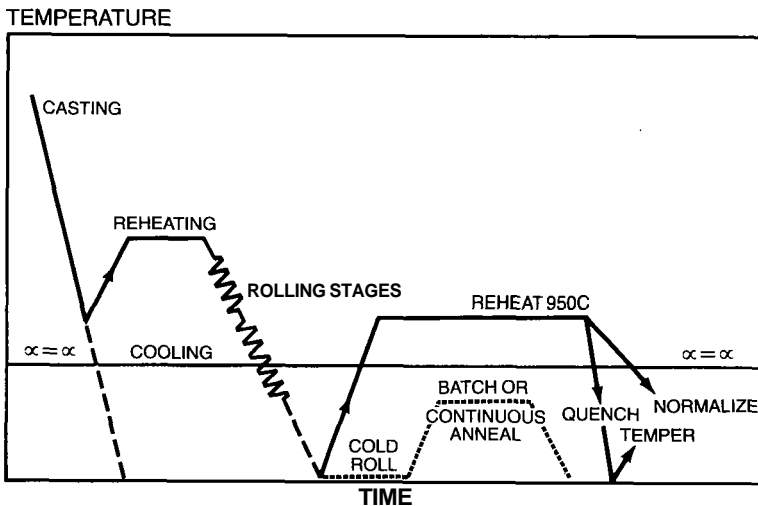


Figure 3 - Summary of processing steps for various products.

## Reheating

The reheated austenite grain size affects the steel's response to thermo-mechanical processing, and for heavy-gauge products it should be as small as possible to maximize impact toughness. The grain size is a function of heating temperature, and time as well as the steel composition, due to its effect on the solubility of grain refining agents, and the prevailing particle size distribution of carbonitride precipitates introduced during solidification and transformation.

There is substantial literature which documents the marked influence of Nb on the behavior of austenite during reheating (16, 24-30). Representative examples are reproduced in Figures 4 through 6. For most steels, the average grain diameter is approximately 20 to 50  $\mu$  at the temperature used for conventional normalizing and quenching and tempering treatments (925-950 C) and 50 to 450  $\mu$  at normal reheating furnace temperatures (1025-1300 C). When more rapid heating rates are used, such as occur in the induction treatment of plate or pipe and the continuous annealing of sheets, the austenite grain sizes may be much finer especially at short times and high temperatures (> 1175 C), (31) Figure 7.

## Rolling

Niobium refines austenite grains by its action in slowing recovery and recrystallization processes and by retarding grain growth after intermediate recrystallizations. In this latter regard Nb is much more effective than vanadium which is relatively soluble, but it is somewhat inferior to titanium, Figure 9 (29).

The processing of niobium-containing austenites has been extensively studied, particularly for steels with low carbon contents, (8-16, 32) but interesting results have also been obtained for high carbon (0.60%) bar steels (33). The magnitude of the effects attributable to niobium are illustrated by the examples in Figures 8-11, (16, 34). Interrelationships exist among niobium solute level, grain size and deformation temperature, Figures 12 and 13 (28). Recent trends to slightly higher niobium contents (0.06-0.10%) in plate products reflect the advantages gained from the lower processing sensitivity of these steels, (35, 36).

For sheet steels, the metallurgical objectives are less related to austenite and ferrite grain refinement (no toughness requirement), and are more concerned with benefits related to precipitation hardening and development of anisotropy. The planar anisotropy results from the combined influence on grain shape and changes in crystallographic texture, (37) and may be usefully employed to intensify the influence of subsequent processing by cold rolling and annealing. In general, the texture exhibited by the ferrite which transforms from unrecrystallized austenite is  $\{112\} \langle 110 \rangle$ , and this texture can be intensified by a decrease in the rolling temperature and an increase in the cooling rate after rolling. This latter effect is due to a lowering of the  $\gamma$ -to- $\alpha$  transformation temperature and a lesser opportunity for recovery or recrystallization of the austenite to occur. Thus, to obtain optimum forming properties in cold-rolled niobium steels, it is essential to first control hot-rolling conditions (38) and coiling temperatures (39).

For hot-rolled steel, precipitation hardening is maximized when niobium is in solution in austenite at the time of transformation to ferrite (40).

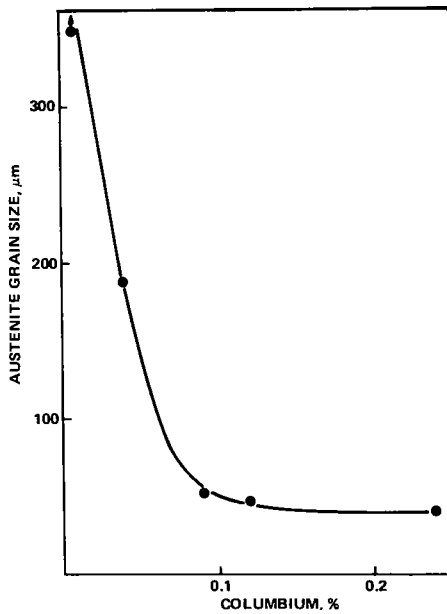


Figure 4 - Effect of columbium content on austenite grain size at 1175 C (2150 F) soak temperature. After Chilton & Roberts (25).

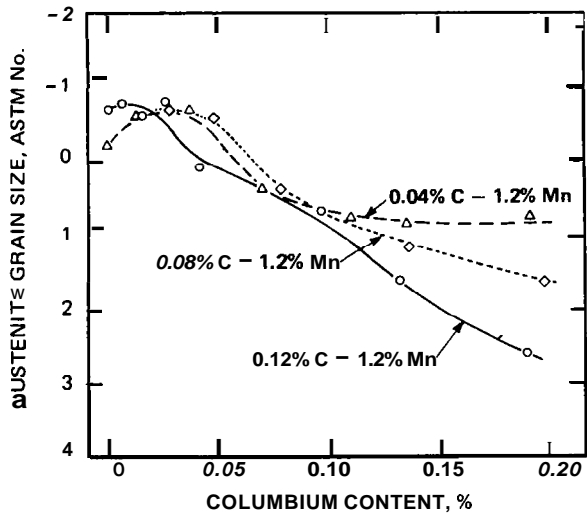


Figure 5 - Effect of columbium on austenite-grain size of three base compositions reheated to 1250 C for 1 hour. After Kozasu et al (16).

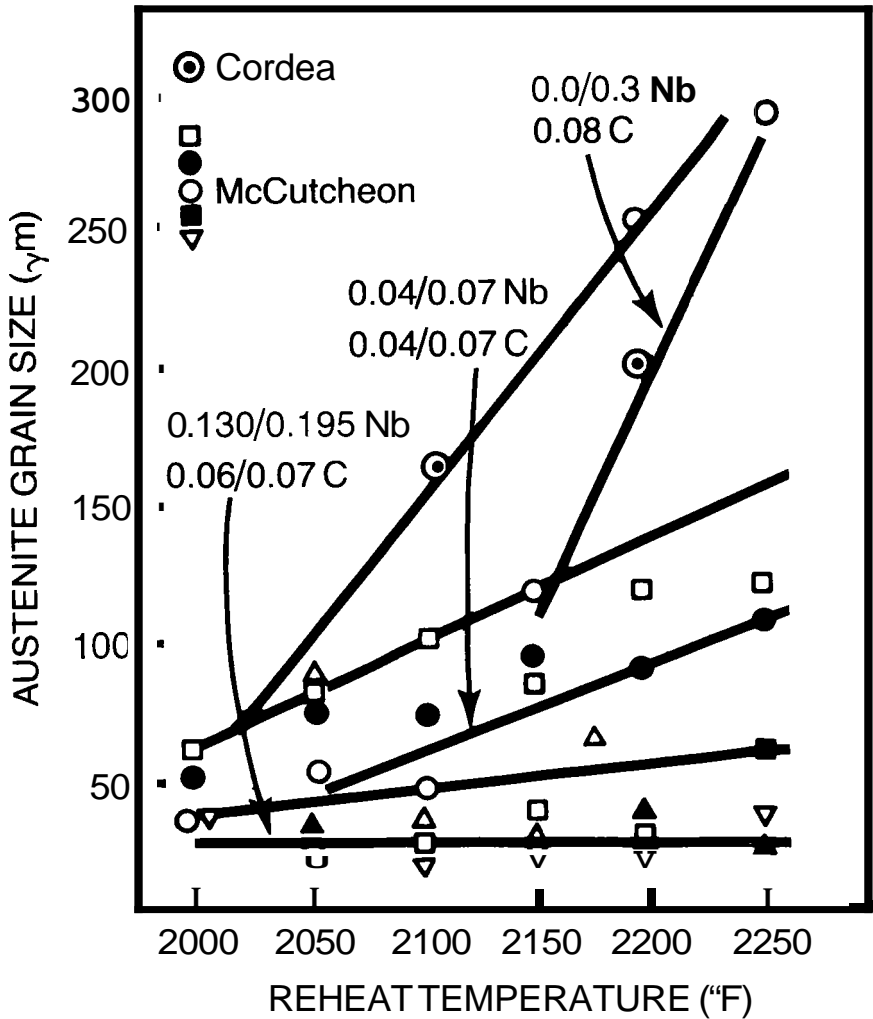


Figure 6 - Effect of reheat temperature on the austenite grain size of niobium bearing steels. After McCutcheon (30).

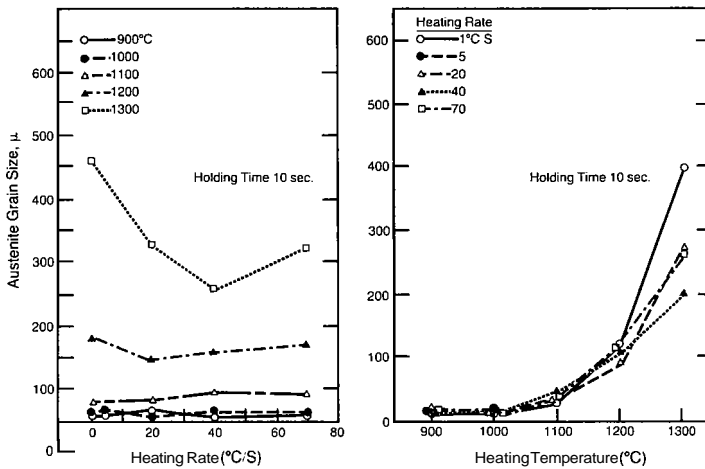


Figure 7 - Effect of reheating rate and reheating temperature on the austenite grain size of a 0.11 percent C, 0.30 si, 0.04 Al, 1.32 Mn, 0.03 Nb, 0.009 N steel after hot rolling. After Ohtani et al (31).

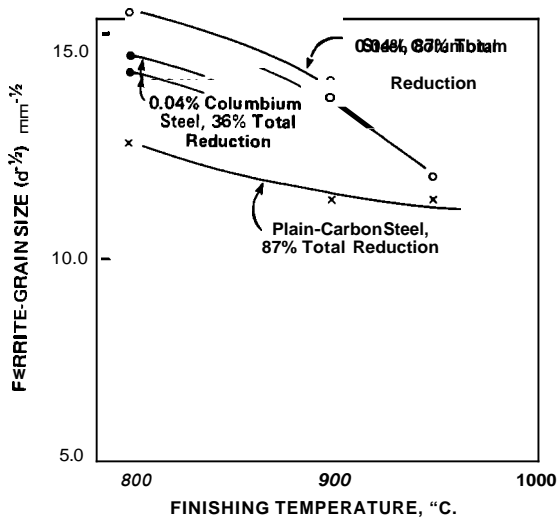


Figure 8 - The effect of finishing temperature, columbium addition, and total reduction on the ferrite-grain size of a 0.17 percent carbon, 1.6 percent manganese steel with and without 0.04 percent columbium. The steel was rolled to a 20-mm diameter bar and air cooled. After Gladman et al (34).

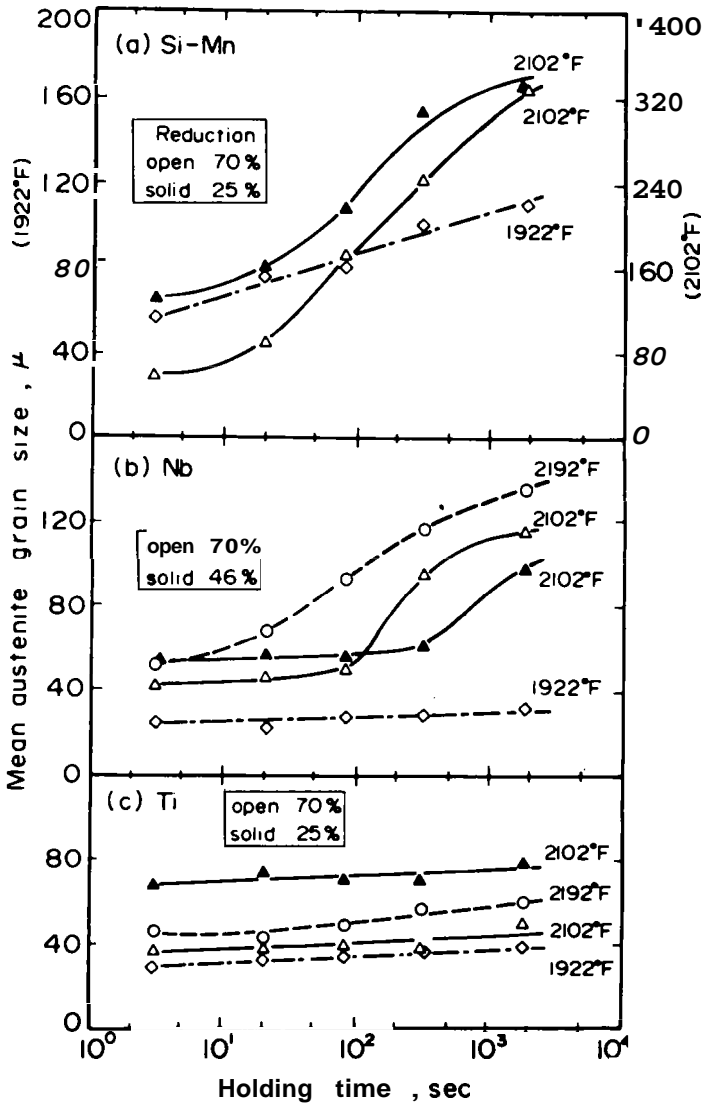


Figure 9 - Grain growth behavior after hot rolling (a) Si-Mn steel (b) Nb steel and (c) Ti steel. After Ouchi et al (29).

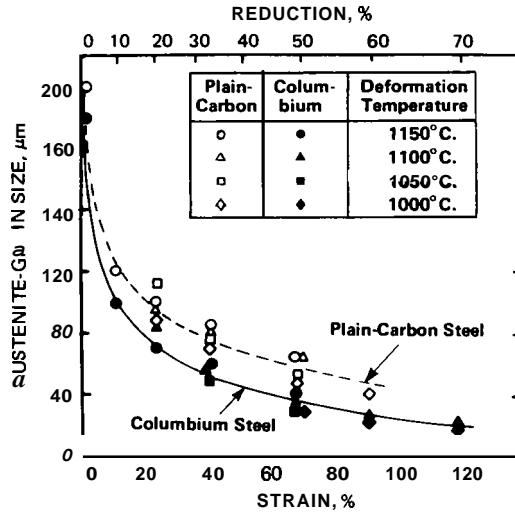


Figure 10 - Influence of the amount of single-pass deformation and the deformation temperature on recrystallized-austenite grain size in plain-carbon and columbium steels. After Tanaka et al (28).

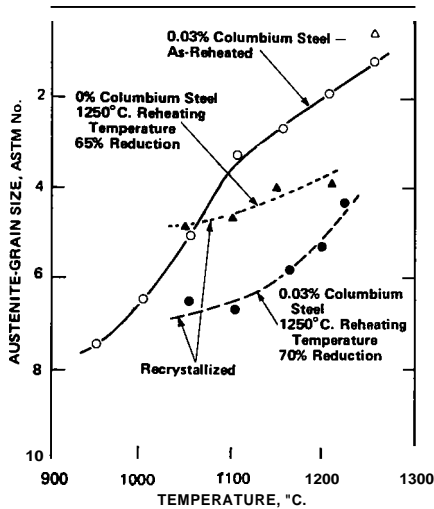


Figure 11 - Effect of columbium on recrystallized grain size after hot rolling with one pass. The columbium-free and 0.03 percent columbium steels have the same base composition. After Kozasu et al (16).

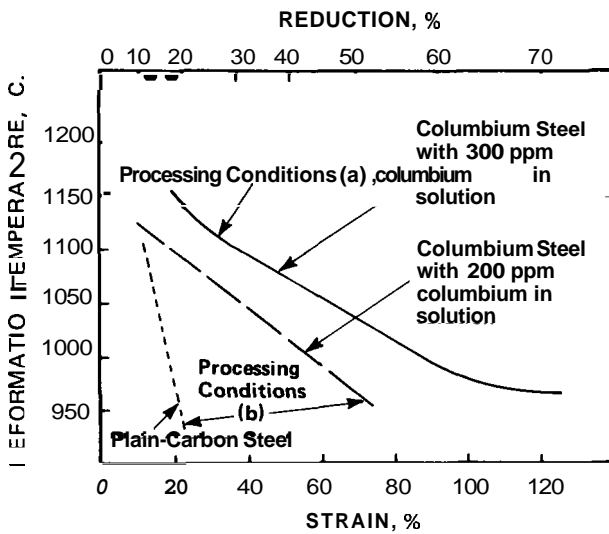


Figure 12 - Effect of dissolved columbium content and deformation temperature on critical amount of deformation required for completion of recrystallization in the plain-carbon and columbium steels. Processing conditions: (a) solution treated for 60 minutes at 1150 C, air cooled to the deformation temperature, rolled by the amount indicated and water quenched; (b) same as (a) but held for 30 minutes at the deformation temperature prior to rolling. After Tanaka et al (28).

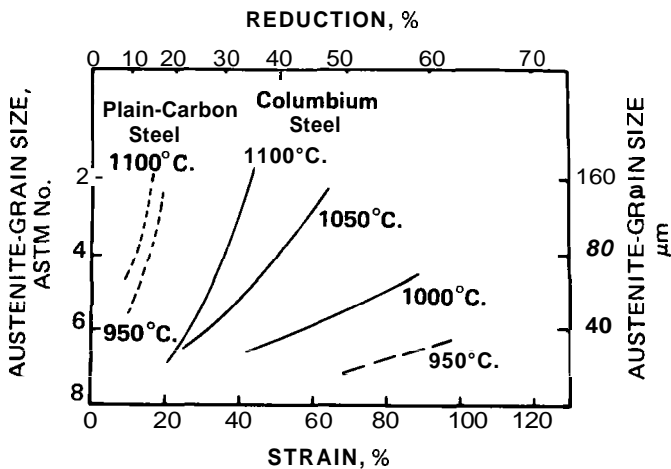


Figure 13 - Effect of deformation temperature and initial grain size on critical amount of deformation required for completion of recrystallization in the plain-carbon and columbium steels. After Tanaka et al (28).

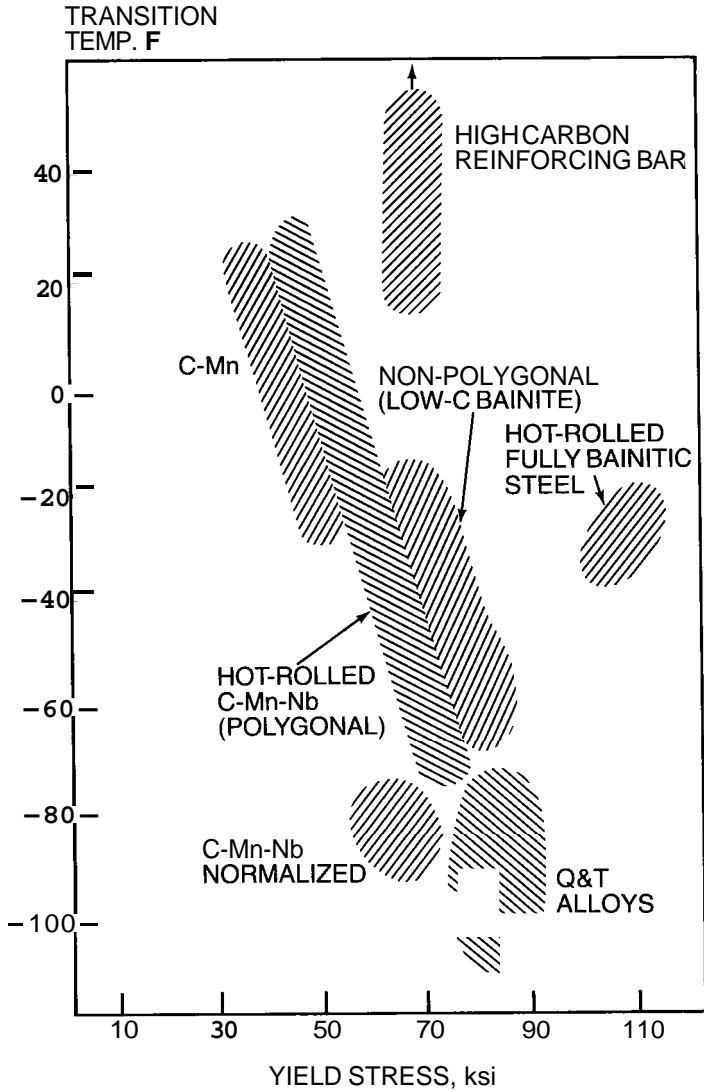


Figure 14 - Properties attainable in various types of steel.

Since premature precipitation is minimized at high-finish rolling temperatures, it is often possible to find increases in yield strength when reheating and finishing temperatures are raised (41). It should be noted that this is the inverse of the relationship usually observed for plate or other heavy-gauge product.

### Cooling

The final properties of hot-rolled production are directly related to conditions of transformation from austenite-to-ferrite and to the precipitation reactions taking place during and after transformation. As required yield strengths increase or product thicknesses increase, it becomes increasingly difficult to achieve appropriate conditions of transformation. Under these conditions, selections have to be made among additional alloying with manganese, molybdenum, boron and other suitable elements or the use of some form of artificial cooling is used usually involving water.

One unusual approach to strengthening involved a process which may be termed "interphase grain refinement", whereby pre-existing carbonitride particles or precipitates occurring during transformation provide additional ferrite grain refinement for any given starting austenite grain size. This phenomenon was first observed by Webster (42) in niobium steels and has recently been mentioned by Woodhead (43) in vanadium microalloyed steel.

### Subsequent thermal treatments

Heat treatment may follow rolling and in such cases niobium acts as a grain refiner and toughener as mentioned earlier. The grain refining effects may be enhanced by proper control of the prior rolling practice as described by other authors at this conference, (44, 45). Recent more novel developments include simultaneous rolling and either intercritical or supercritical "normalizing" treatments (SHT process (46)), and here again niobium enhances the grain refining potential of the deformation process.

### Properties obtained

The range of mechanical properties attainable in various types of niobium steel are summarized in Figures 14 and 15. The individual types of steel are discussed in detail elsewhere in this volume. Since the production of microalloyed steels is relatively non-energy intensive compared with heat-treated steels, it is expected that the importance of these products will grow as energy costs continue to escalate during the coming years.

## Fundamental Considerations

### Electronic structure

Iron, manganese and niobium belong to the family of metallic elements known as transition metals. Transition metals are characterized by the electronic structure of the atoms where the outer shell (4s energy level for period 4 and 5s for period 5 elements) contain electrons while the inner shell (3d energy level for period 4 and 4d for period 5 elements) is not

completely filled. The transition metals are the only elements that have unfilled inner shells. Many of the elements that form substitutional solid solutions with iron in HSLA steels are shown in Table I, (47).

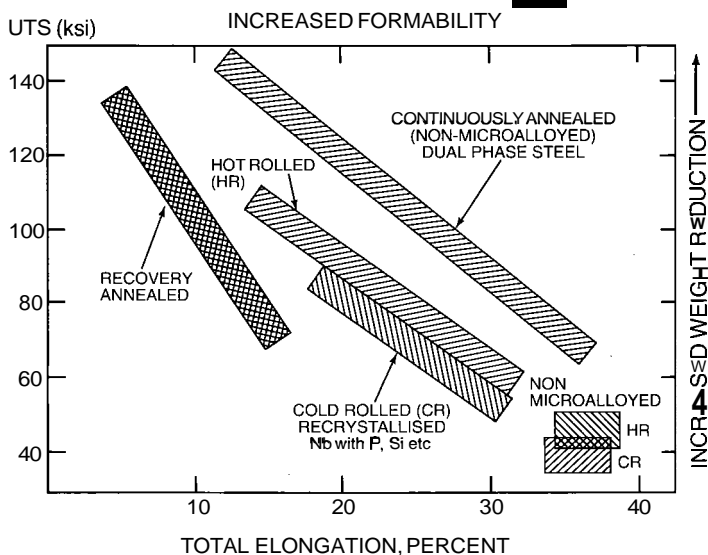


Figure 15 - Properties attainable in sheet and strip.

Fe-Nb phase diagram

As might be expected from the crystallographic data, niobium and iron are completely miscible at high temperatures. The equilibrium diagram for the iron-niobium system is well established: details may be found in standard texts, (48). The most interesting feature of the diagram, in relation to the use of niobium in steels, is the existence of a  $\gamma$  loop which limits the existence of the  $\gamma$  phase to alloys containing less than 0.83 percent niobium (0.50 at. %). Clearly, niobium is a ferrite stabilizer. However, additions of up to 0.10 to 0.20 percent lower the  $A_3$  temperature, i.e., the  $\gamma$  loop apparently displays a minimum similar to that observed in the iron-chromium and iron-vanadium systems; thus, in small quantities niobium acts as a  $\gamma$  stabilizer.

In the ternary iron-carbon-niobium system, the major feature of the equilibrium diagram relevant to steels is the marked reduction of the solubility of carbon in austenite and ferrite as a result of the ready formation of niobium carbide.

Diffusion

The literature contains several estimates of the interdiffusion coefficients in dilute solutions of niobium in  $\gamma$  iron, (49-52). The data show considerable scatter and are considered unreliable.

Table I. Abbreviated Periodic Table Showing Some of the Elements Which Form Solid Solutions with Iron.\*

IV B		V B		VI B		VII B		VIII			I B		II B													
22 47.90 <b>Ti</b> Titanium 4.5 3130 1812 (Ar) 3d <sup>2</sup> 4s <sup>2</sup>	23 50.94 <b>V</b> Vanadium 5.96 3530 1730 (Ar) 3d <sup>3</sup> 4s <sup>2</sup>	24 52.00 <b>Cr</b> Chromium 7.1 2482 1903 (Ar) 3d <sup>4</sup> 4s	25 54.94 <b>Mn</b> Manganese 7.2 2087 1244 (Ar) 3d <sup>5</sup> 4s	26 55.85 <b>Fe</b> Iron 7.86 2800 1535 (Ar) 3d <sup>6</sup> 4s	27 58.93 <b>Co</b> Cobalt 8.9 2900 1490 (Ar) 3d <sup>7</sup> 4s <sup>2</sup>	28 58.71 <b>Ni</b> Nickel 8.9 2800 1455 (Ar) 3d <sup>8</sup> 4s <sup>2</sup>	29 63.54 <b>cu</b> Copper 8.9 2310 1083 (Ar) 3d <sup>10</sup> 4s	30 65.37 <b>Zn</b> Zinc 7.14 907 419.5 (Ar) 3d <sup>10</sup> 4s <sup>2</sup>	40 91.22 <b>Zr</b> Zirconium 6.4 3580 1852 (Kr) 4d <sup>2</sup> 5s <sup>2</sup>	41 92.91 <b>Nb</b> Niobium 8.4 3300 1950 (Kr) 4d <sup>4</sup> 5s	42 95.94 <b>Mo</b> Molybdenum 10.2 4804 2610 (Kr) 4d <sup>5</sup> 5s (Kr) 4d <sup>5</sup> 5s <sup>2</sup>	43 (98) <b>Tc</b> Technetium 11.4872200 (Kr) 4d <sup>5</sup> 5s <sup>2</sup> (Kr) 4d <sup>5</sup> 5s <sup>2</sup>	44 101.1 <b>Ru</b> Ruthenium 12 1902 77	45 102.905 <b>Rh</b> Rhodium 12.4 1922 78	46 106.4 <b>Pd</b> Palladium 11.98 1950 9	47 107.870 <b>Ag</b> Silver 10.5 1950 961 (Kr) 4d <sup>10</sup> 5s	48 112.40 <b>Cd</b> Cadmium 8.6 767 321 (Kr) 4d <sup>10</sup> 5s <sup>2</sup>	72 178.49 <b>Hf</b> Hafnium 13.30 3230 2230 (Xe) 4f <sup>14</sup> 5d <sup>2</sup> 6s <sup>2</sup>	73 180.95 <b>Ta</b> Tantalum 16.6 6000 2977 (Xe) 4f <sup>14</sup> 5d <sup>3</sup> 6s	74 183.85 <b>W</b> Tungsten 19.3 5630 3380 (Xe) 4f <sup>14</sup> 5d <sup>4</sup> 6s	75 186.2 <b>Re</b> Rhenium 21.0 3147 (Xe) 4f <sup>14</sup> 5d <sup>5</sup> 6s	76 186.2 <b>Os</b> Osmium 22.48 4400 2700	77 192.2 <b>Ir</b> Iridium 22.4 4350 2443 (Xe) 4f <sup>14</sup> 5d <sup>6</sup> 6s <sup>2</sup>	78 195.09 <b>Pt</b> Platinum 21.45 4010 1770 (Xe) 4f <sup>14</sup> 5d <sup>9</sup> 6s	79 196.97 <b>Au</b> Gold 19.3 2660 1063 (Xe) 4f <sup>14</sup> 5d <sup>10</sup> 6s	80 200.59 <b>Hg</b> Mercury 13.546 3568 -3887 (Xe) 4f <sup>14</sup> 5d <sup>10</sup> 6s <sup>2</sup>

KEY	
Atomic number	* Atomic weight
<b>Atomic symbol</b>	
Name of element	
density (g/ml)	
BP °C	MP °C
Ground state symbol (electronic configuration)	

**EXPLANATION**  
 \* in ( ) = mass number of the most stable isotope  
 Atomic symbols cross-hatched as Br and Hg = liquids at 25°C  
 Atomic symbols outlined as He, Ne, etc. = gases

\* After Smith (47).

Recently Argentinian investigators (53) have studied the diffusion of niobium in high-purity iron containing no detectable interstitial levels. Fe, Fe-0.4 Si and Fe-0.6 Si-1.5 Mn alloys were investigated at temperatures > 1080 C. The experiments were conducted using the radioactive tracers Nb<sup>95</sup> and Nb<sup>96</sup>, and the concentration profiles were determined by direct sectioning. The interdiffusion coefficients of Nb in austenite in various iron-based alloys are shown in Figure 16. Two important observations emerge: firstly, that the interdiffusion coefficient of Nb in austenite is not strongly influenced by the composition of the solid solution matrix, and, secondly, that the coefficient for Nb is somewhat higher than the coefficient for the self-diffusion of iron.

### Compound Forming Tendencies

Transition metals are known to form a series of simple and solid solution compounds of oxides, sulfides, carbides and nitrides. The compound forming tendencies of several of the transition metals in steel have been reviewed recently (54, 55) and have been summarized by Meyer, et al, (56), Figure 17. Niobium shows a strong tendency to form carbonitrides, but relatively little tendency to form oxides, sulfides or solid solutions of these compounds. In this regard it behaves similarly to vanadium.

This characteristic distinguishes it from titanium which does not act as a carbide former until all oxygen, nitrogen and sulfur have been consumed by initial additions of titanium.

### Precipitation of Niobium Compounds: Nb-NbC System

The Nb-NbC system has been studied extensively over the last quarter century, (57, 62) the most recent and definitive study being that of Storms and Krikorian, (62). The Nb-NbC phase diagram is shown in Figure 18. There are three solid-solution, single-phase regions: a, β and γ. The a-phase is

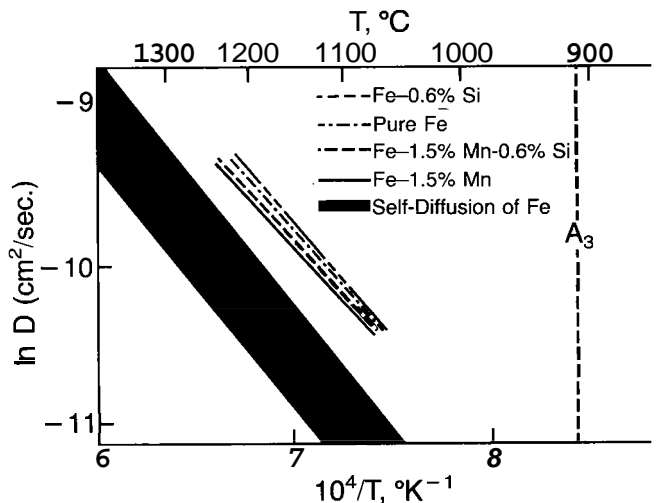


Figure 16 - Interdiffusion coefficients of niobium in interstitial-free substitutional alloys.

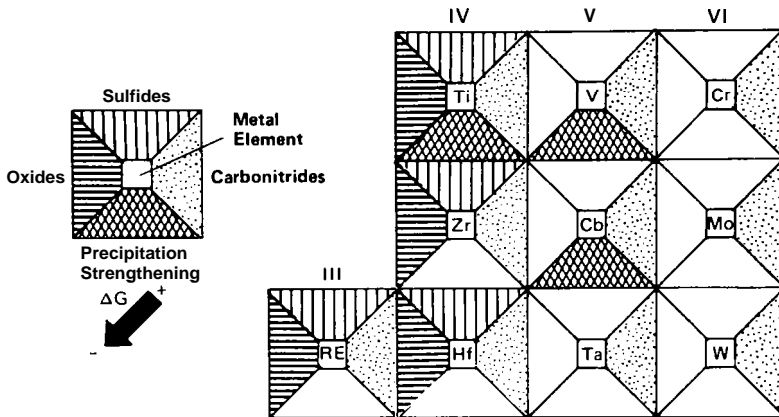


Figure 17 - The tendency of certain metals to form oxides, sulfides, carbides, and nitrides and their precipitation-strengthening potential (arranged similar to the periodic table). After Meyer et al (56).

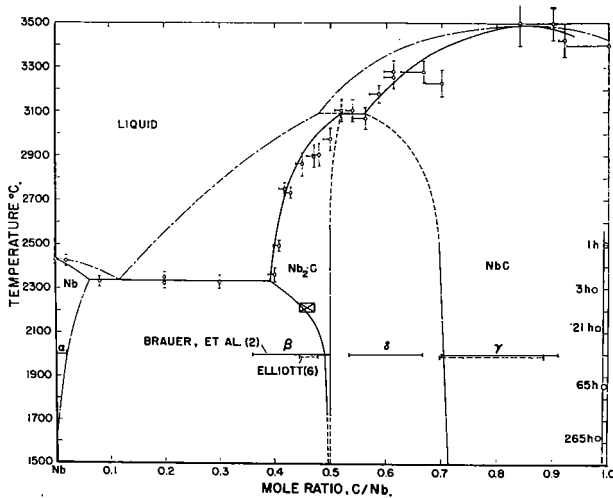


Figure 18 - Niobium-niobium carbide phase diagram. After Storms and Krikorian (59).

an interstitial solid solution of carbon in Nb, with a maximum solid solubility of **0.2** at. percent C near **2300** C. A vanishingly small carbon solid solubility would be expected at temperatures of interest in steelmaking. The  $\alpha$ -phase has an A2 (BCC) crystal structure with a lattice parameter that will vary with the carbon content and is **3.2948** for pure Nb, (57). The  $\beta$ -phase ( $\text{Nb}_2\text{C}$ ) also appears to have a very limited range of carbon solubility around the stoichiometric composition (**33.3** at. % C) below **1500** C.  $\text{Nb}_2\text{C}$  has an HCP crystal structure with lattice parameters  $a = \mathbf{3.128}$  and  $c = \mathbf{4.95}$ , (57). The phase of the Nb-NbC system that is of most interest in steels is the  $\gamma$ -phase "NbC", but it should be noted that  $\text{Nb}_2\text{C}$  is observed in steels having high Nb/C ratios, (63). The  $\gamma$ -phase has a range of carbon solubility which, for example, appears to extend from near  $\text{NbC}_{.72}$  to NbC at **1100** C. This range of possible carbon contents has led to the adoption of the symbol NbC to describe the  $\gamma$ -phase, with x being equal to the mole ratio of C to Nb (at **1100** C; therefore,  $\mathbf{0.72} \leq x \leq \mathbf{1.0}$ ). The  $\gamma$ -phase  $\text{NbC}_x$  has a **B1** (NaCl) type [FCC] crystal structure (64) whose symmetry is described by the Schoenflies point group  $O_h^5$  and Hermann-Mauguin space group (shortened)  $Fm\bar{3}M$  with 8 atoms per unit cell. The crystal structure of NbC can be represented by two interpenetrating FCC lattices with Nb atoms (or Nb atom vacancies) residing on one set of FCC lattice points and C atoms (or C atom vacancies) residing on the other set.  $\text{NbC}_x$  can be considered, therefore, to consist of Nb atoms, C atoms and vacancies. If we let  $N^o$  equal the number of atom positions on either FCC lattice containing Nb or C atoms, then we have the following relationship:

$$N^o = N_{\text{Nb}} + N_{\text{Nb}}^v = N_{\text{C}} + N_{\text{C}}^v \quad (1)$$

where

$N_{\text{Nb}}$  = no. Nb atom sites per unit volume containing an Nb atom

$N_{\text{Nb}}^v$  = no. vacant Nb atom sites per unit volume

$N_{\text{C}}$  = no. C atom sites per unit volume containing a C atom

$N_{\text{C}}^v$  = no. vacant C atom sites per unit volume.

Subtracting  $N_{\text{Nb}}^v$  from both sides we get

$$N_{\text{Nb}} = N_{\text{C}} + (N_{\text{C}}^v - N_{\text{Nb}}^v) \quad (2)$$

Since, by convention, the subscript of the Nb is taken as one, both sides of equation (2) should be divided by  $N_{\text{Nb}}$ . This gives

$$1 = \frac{N_{\text{C}}}{N_{\text{Nb}}} + \frac{N_{\text{C}}^v - N_{\text{Nb}}^v}{N_{\text{Nb}}} \quad (3)$$

$$\text{where } \frac{N_C}{N_{Nb}} = x \text{ in NbC}_x, \quad (3a)$$

$$\text{and } \frac{N_C^V - N_{Nb}^V}{N_{Nb}} = 1 - x \quad (3b)$$

Equations (3) indicate that if the number of vacancies on Nb and C sites is equal, then  $N_{Nb} = N_C$  and  $x$  in  $\text{NbC}_x$  would be equal to one and the carbide would have the stoichiometric composition. If, however, there are more vacancies in the carbon lattice, then  $N_{Nb} > N_C$  and  $x < 1.0$ ; this, of course, is the usual case. It can be concluded, therefore, that there is a direct relationship between the deviation in  $x$  from  $x = 1$  and the vacancy concentration in  $\text{NbC}_x$ .

The lattice parameter of  $\text{NbC}_x$  has been shown to be a strong function of  $x$ , Figure 19, (62). Pure, stoichiometric NbC has a lattice parameter of 4.470Å and the lattice parameter decreases with decreasing  $x$  to a value of about 4.43Å at  $\text{NbC}_{.7}$ . Clearly, the vacancy concentration in the  $\gamma$ -phase has a very strong influence on the lattice parameter.

Microalloyed steels contain both carbon and nitrogen and when niobium precipitates it does so as niobium carbonitride, (65-69). The crystallography of "NbC" has been discussed above and, in fact, is very similar to "NbN", (64). Since "NbC" and "NbN" are very similar compounds, it is quite reasonable to expect the two to have complete solid solubility, i.e. form a carbonitride. This is, in fact, correct, (70).

The NbC-NbN system has been studied (71, 72) and reviewed, (62). The NbC-NbN system is actually a ternary system of NbC, NbN and vacancies. This ternary system and associated lattice parameters are shown in Figure 20. Two very important points emerge from an inspection of Figure 20. First, the composition of niobium carbonitride can be represented by  $\text{NbC}_x\text{N}_y$  where  $x$  equals the mole ratio of C/Nb,  $y$  equals the mole ratio of N/Nb and  $1 - (x + y)$  equals the mole ratio of vacancies. Figure 20 also indicates that the quantities  $x$ ,  $y$  and  $(x + y)$  can all be variables. Second, the lattice parameters of the carbonitride will be strongly influenced by both the nitrogen and vacancy concentration; both nitrogen and vacancies act to reduce the lattice parameter of pure NbC. Figure 20 further illustrates that the extent to which the lattice parameter is lowered with increased nitrogen will depend on the vacancy concentration of the carbonitride. The higher the vacancy concentration, the larger will be the lowering of lattice parameter per unit increase in nitrogen content in the carbonitride. Storms and Krikorian point out that the interpretation of lattice parameter measurements will be difficult unless the vacancy concentration in the carbonitride can be assessed, (62).

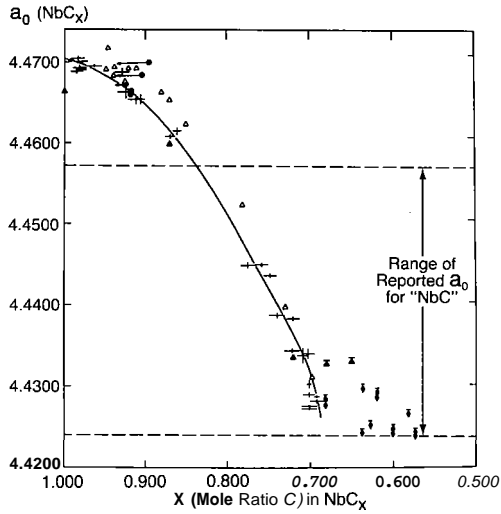


Figure 19 - Variation of NbC lattice parameter with composition. After Storms and Krikorian (59).

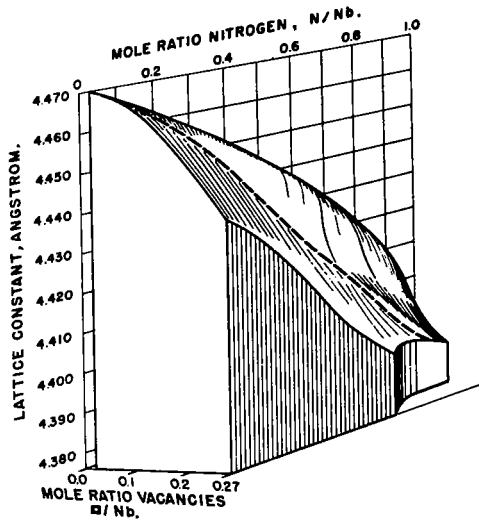


Figure 20 - Lattice parameter versus composition in the system NbN-NbC. After Storms and Krikorian (59).

## Composition of NbC<sub>x</sub>N<sub>y</sub> Formed in Niobium Steels

The composition of precipitates found in commercial steels has been extensively studied and the results obtained prior to 1973 were reviewed by Gray, (73).

Briefly, it can be stated that the cubic forms of carbonitride are most frequently found at normal niobium levels (< 0.04%). The reported range of stability from NbC<sub>0.72</sub> to NbC<sub>1.0</sub> (74, 75) may allow substitution of molybdenum (76, 77) as well as the nitrogen/vacancy contents discussed earlier without causing changes in crystal structure.

Recent studies of the composition of the carbonitride which forms in Nb-bearing microalloyed steels (65-69, 78-80) have shown a direct relationship between the composition of the carbonitride and the composition of the steel; the larger the N/C ratio in the steel, the more nitrogen-rich was the carbonitride. A typical example of the relation is shown in Figure 21, (68).

These and other studies (73, 81-84) have also shown that the composition of the carbonitrides in any given steel can depend upon the thermal conditions under which they form. The data indicate that the precipitates contain more nitrogen when formed at higher temperatures, (52, 67, 69, 84) Figures 22 and 23, (84) which is similar to results for precipitation of vanadium carbonitride in vanadium-strengthened microalloyed steels, (85, 86).

It is to be expected that the presence of other elements such as titanium and aluminum, that have strong nitride-forming tendencies, will affect the amount of nitrogen in W C<sub>x</sub>N<sub>y</sub>. This has been observed by Ouchi, et al., (80) especially in steels austenitized at high temperatures, Figure 24.

These studies (81-83) also indicate that long austenitizing treatments (< 150 h) and higher niobium (< 0.10%) and nitrogen contents (< 0.012%) give rise to the formation of non-cubic compounds, often of the hexagonal 6' or ε carbonitride type. Also, as stated earlier, Nb<sub>2</sub>C-type precipitates are observed at high Nb/C mole ratios (63, 73).

## The Solubility of NbC<sub>x</sub>N<sub>y</sub> in Austenite

The formation (and dissolution) of precipitates normally exhibits sigmoidal kinetic curves which can be approximated by the Johnson-Mehl equation (87).

$$X_p = 1 - \exp \left[ - \frac{\pi}{3} N G^3 t^4 \right] \quad (4)$$

where  $X_p$  = fraction of precipitation formed

$N$  = nucleation rate (usually assumed constant)

$G$  = growth rate (usually assumed constant)

$t$  = reaction time.

The equation shows that a precipitation reaction will attain a given level of completion only when  $N$ ,  $G$  and  $t$  have sufficiently large values. The nucleation rate is controlled by solute supersaturation while the growth rate



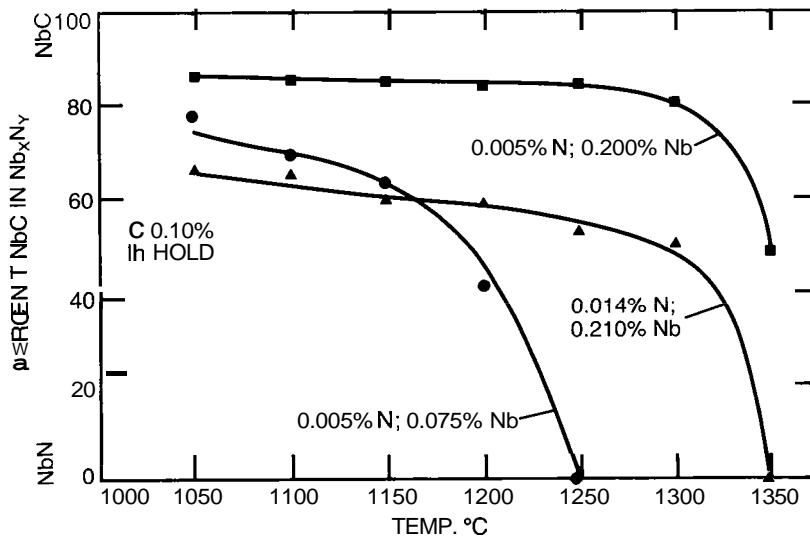


Figure 23 - Change in  $NbC_xN_y$  composition with temperature and niobium content (84).

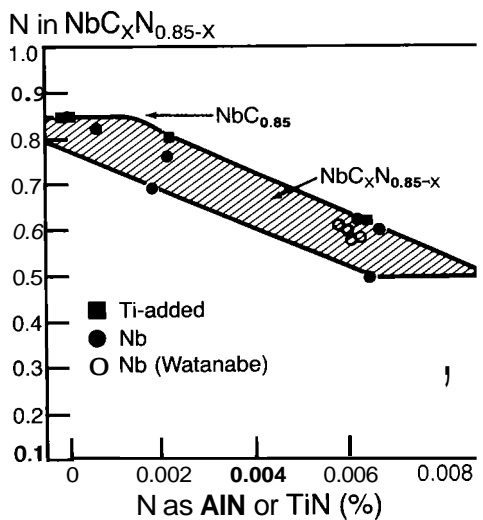


Figure 24 - The relationship between the nitrogen content uncombined with Al or Ti and the composition of niobium carbonitride. After Ouchi (80).

is controlled by both the diffusion coefficient and the solute supersaturation, (88). Since solute supersaturation controls both N and G, it is very important to understand the factors which determine it.

The extent to which elements can be maintained in solid solution in austenite is governed by the appropriate solubility product. If, for example, we are interested in the extent of solid solubility of Nb and C in austenite which is in equilibrium with pure, stoichiometric NbC, then we must consider this reaction



This reaction will have an associated solubility product

$$\log K_1 = \log [\text{Nb}] [\text{C}] = A_1 - \frac{B_1}{T} \quad (6)$$

where  $A_1$  and  $B_1$  are constants normally specified such that  $[\text{Nb}]$  and  $[\text{C}]$  can be expressed in wt. percent and  $T$  in °K. If, however, we wanted to consider the extent of solubility of the austenite in equilibrium with  $\text{NbC}_{.85}$ , then the appropriate solubility product would be:

$$\log K_2 = \log [\text{Nb}] [\text{C}]^{.85} = A_2 - \frac{B_2}{T} \quad (7)$$

Similarly, the solubility product for austenite in equilibrium with  $\text{NbC}_x\text{N}_y$  would be

$$\log K_3 = \log [\text{Nb}] [\text{C}]^x [\text{N}]^y = A_3 - \frac{B_3}{T} \quad (8)$$

The solubility of "NbC" in austenite has been studied in numerous investigations, and this work has been carefully summarized and reviewed by Nordberg and Aronsson, (78). The 13 independent investigations reviewed by Nordberg and Aronsson examined the solubility products associated with NbC,  $\text{NbC}_x$ ,  $\text{NbC}_x\text{N}_y$  and NbN. Several solubility products are illustrated in Figure 25, and the equations of these products are listed in Table II.

Table II, Solubility of Niobium Carbonitride Precipitates in Austenite

<u>Precipitate</u>	<u>Solubility Expression</u>	<u>Reference</u>
NbC <sub>.97</sub>	$\log [\text{Nb}] [\text{C}]^{.87} = 3.43 - \frac{7170}{T}$	78
NbC	$\log [\text{Nb}] [\text{C}] = 2.96 - \frac{7510}{T}$	78
NbC <sub>.83</sub> N <sub>.14</sub>	$\log [\text{Nb}] [\text{C}]^{.83} [\text{N}]^{.14} = 4.46 - \frac{9800}{T}$	79
NbC <sub>.24</sub> N <sub>.65</sub>	$\log [\text{Nb}] [\text{C}]^{.24} [\text{N}]^{.65} = 4.09 - \frac{10,400}{T}$	82
NbN	$\log [\text{Nb}] [\text{N}] = 2.80 - \frac{8500}{T}$	54

The relationship between the solubility product and the nature or composition of the niobium precipitate is evident in Figure 25. If the solubility product line for pure, stoichiometric NbC is used as a reference, two interesting trends are observed. First, there is a substantial lowering of the product as the precipitate becomes more enriched with nitrogen. Second, there is an apparent increase in solubility product with a reduction in x (i.e. with an increase in vacancy content). These two trends are illustrated with a comparison of selected solubility products for several precipitates at 1000 C, as shown in Table III.

Table III. Solubility Product Values at 1000°C

<u>Precipitate</u>	<u>K x 10<sup>6</sup></u>
NbC <sub>.87</sub>	1510
NbC	1070
NbC <sub>.83</sub> N <sub>.14</sub>	525
NbC <sub>.24</sub> N <sub>.65</sub>	77.6
NbN	8.0

Solubility products play a vital role in understanding the physical metallurgy of microalloyed steel, especially those aspects which are concerned with precipitation-related phenomena. Solubility products can be plotted in either of two ways. Consider the case of the solubility product of NbC in austenite at some given temperature. If the abscissa (C) and ordinate (Nb) axes have a linear scale, then any given solubility isotherm will have the shape of a hyperbole. If, however, the axes have a logarithmic scale, then the solubility isotherm will be a straight line. Both approaches have been widely used in the literature.

A hypothetical solubility isotherm for NbC in equilibrium with austenite at 1000 C is shown in Figure 26(a). The solubility isotherm gives the locus of Nb and C products which represents the limit of solid solubility of NbC in austenite at 1000 C, i.e. any combination of products located above the line will be in the  $\gamma + \text{NbC}$  phase field at 1000 C. The straight line with a positive slope on the diagram represents the stoichiometric ratio. The precipitation of NbC can be followed by considering the slightly curved line which is nearly equidistant from the stoichiometric line and passes through the point with the Nb and C coordinates which describe the composition of the steel. A schematic illustration is presented in Figure 26(b). Consider a steel of composition given by point B which is reheated to 1300 C and is very slowly cooled to 900 C. Since 1300 C is the solution temperature for the NbC under consideration here, the NbC can be assumed to be completely dissolved after reheating. If we further assume that precipitation occurs during the cooling, then the composition of the austenite in equilibrium with NbC would move along the curve passing through point B and which is equidistant from the stoichiometric line. The distance moved along the curved line through point B is proportional to the volume fraction of precipitate formed as a result of the cooling, assuming equilibrium is established at all temperatures. In other words, the distance moved along the curved line through B during cooling is proportional to the supersaturation and would also be proportional

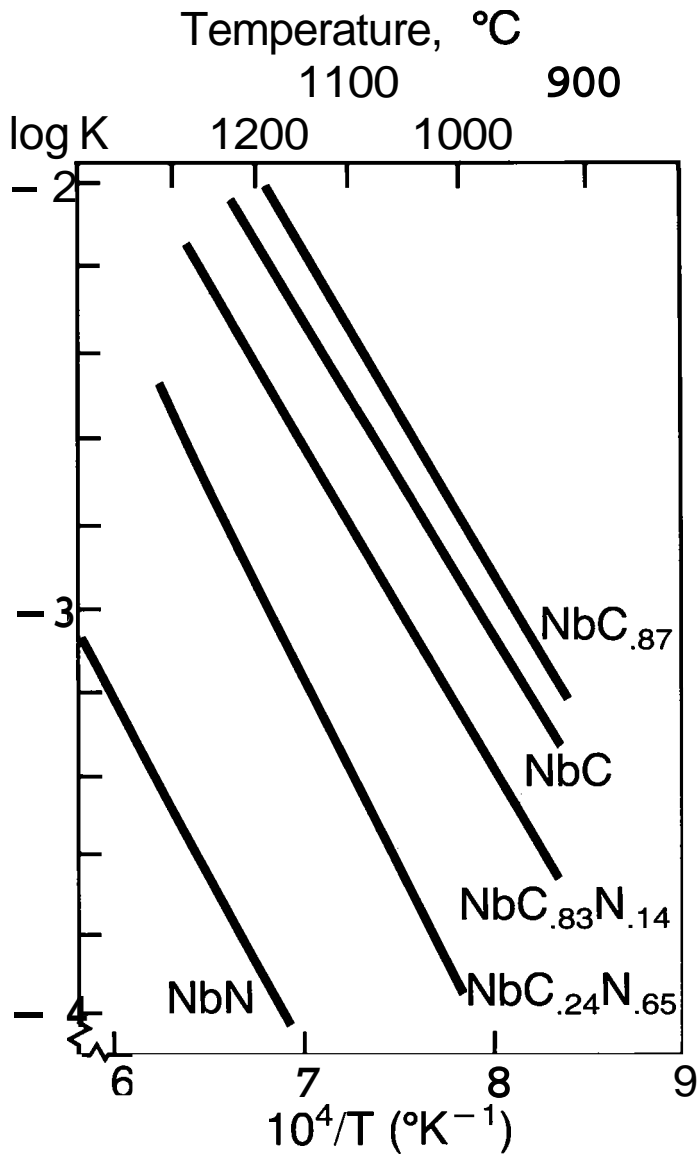
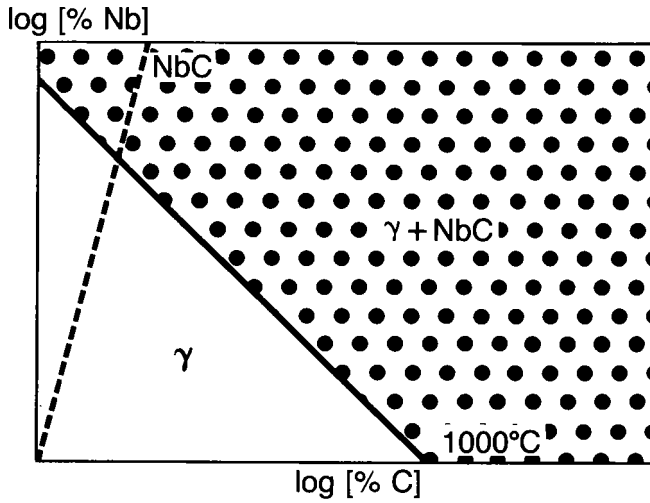
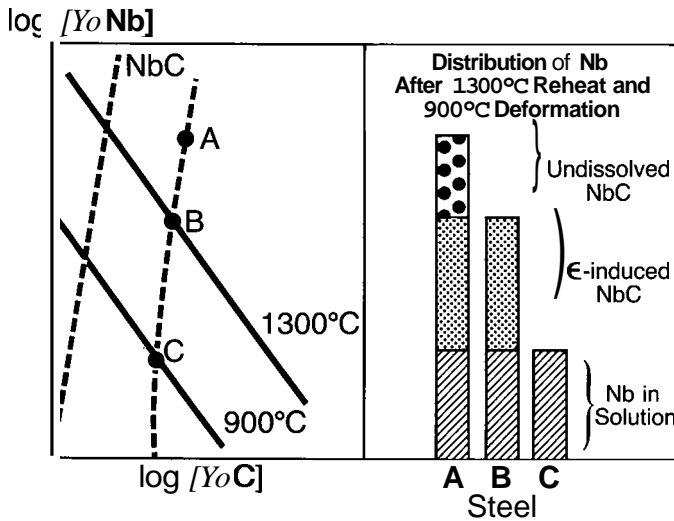


Figure 25 - Solubility products for various Nb precipitates in austenite. After Nordberg and Aronson (78).



(a)



(b)

Figure 26 - Hypothetical solubility diagrams describing equilibrium between NbC and austenite: (a) relationship at 1000 C and (b) interrelationships among isotherms, steel composition, processing and potential amount of precipitation.

to the volume fraction precipitate formed if equilibrium prevailed. Therefore, if steel B is reheated to 1300 C and then cooled to and rolled at 900 C, the distance  $\overline{BC}$  in Figure 26(b) will be proportional to the volume fraction of precipitation of NbC formed in austenite. This precipitation would be of two types: that formed during cooling and that formed during or after rolling. The first type is not likely to be significant since precipitation in recrystallized austenite is normally very sluggish, as will be discussed later. The second type is the strain-induced precipitation. A second interesting case would occur if steel of composition A in Figure 26(b) is considered. If this steel is reheated at 1300 C and hot rolled at 900 C, then two arrays of NbC particles would be expected. The first would be the precipitates that survived the reheating treatment (volume fraction proportional to  $\overline{AB}$ ) and the second strain-induced precipitate (volume fraction proportional to  $\overline{BC}$ ).

Several investigators have used solubility diagrams to help explain the physical metallurgy of microalloyed steels, and, in particular, the precipitation phenomena, (34, 89). Our understanding of precipitation in these steels has been substantially increased by recent work by Wadsworth, et al, (90) Roberts, et al., (85) and Keown and Wilson, (91). The study by Wadsworth, et al., (90) concluded that the supersaturation that could be developed between any two temperatures is a strong function of the position of the steel relative to precipitate stoichiometry on the solubility diagram. This effect, illustrated in Figure 27, shows that the largest possible supersaturation occurs when the microalloying element and the interstitial are present in the steel in the stoichiometric ratio, and deviations from this ratio will lead to decreasing supersaturations.

The work of Roberts, et al., (85) presents an interesting way of considering the precipitation of carbonitride precipitates in microalloyed steels. They suggest a thermodynamic analysis which attempts to predict the change of  $x$  and  $y$  in  $VC_xN_y$ , with changes of temperature and/or extent of precipitation. Their model predicts that nitrogen-rich precipitates are the first to form and that nitrogen plays a central role in controlling the precipitation until it is completely consumed.

Keown and Wilson (91) have suggested a way of analyzing the supersaturations that can develop in steels which contain the potential for formation of several types of precipitates (e.g. NbN - vs - AlN). The technique developed by Keown and Wilson centers on the formation of so-called "equal solubility diagrams" which are constructed from the solubility diagrams of the different precipitating species being considered. In those cases when precipitation kinetics would be governed by solute supersaturation, the location of a given steel on the equal solubility diagram will enable the prediction of the precipitate which is most likely to be formed, i.e. the one with the highest supersaturation. An example of the diagram concerned with NbN and AlN precipitation is shown in Figure 28.

The lines on the diagram represent the loci of Nb and Al compositions where NbN and AlN have equal solubility at a given temperature. Keown and Wilson contend that, for example, steel compositions which lie above one of the lines would favor NbN as the first precipitate to form. As precipitation proceeds, the Nb level in solution in the austenite will fall until it reaches the line of equal solubility, at which point the precipitation of NbN and AlN would be equally favored. For example, if the precipitation in a steel containing .06 Nb and .02 Al is to be studied at, say, 900 C, the steel composition lies above the line of equal solubility for 900 C. This means

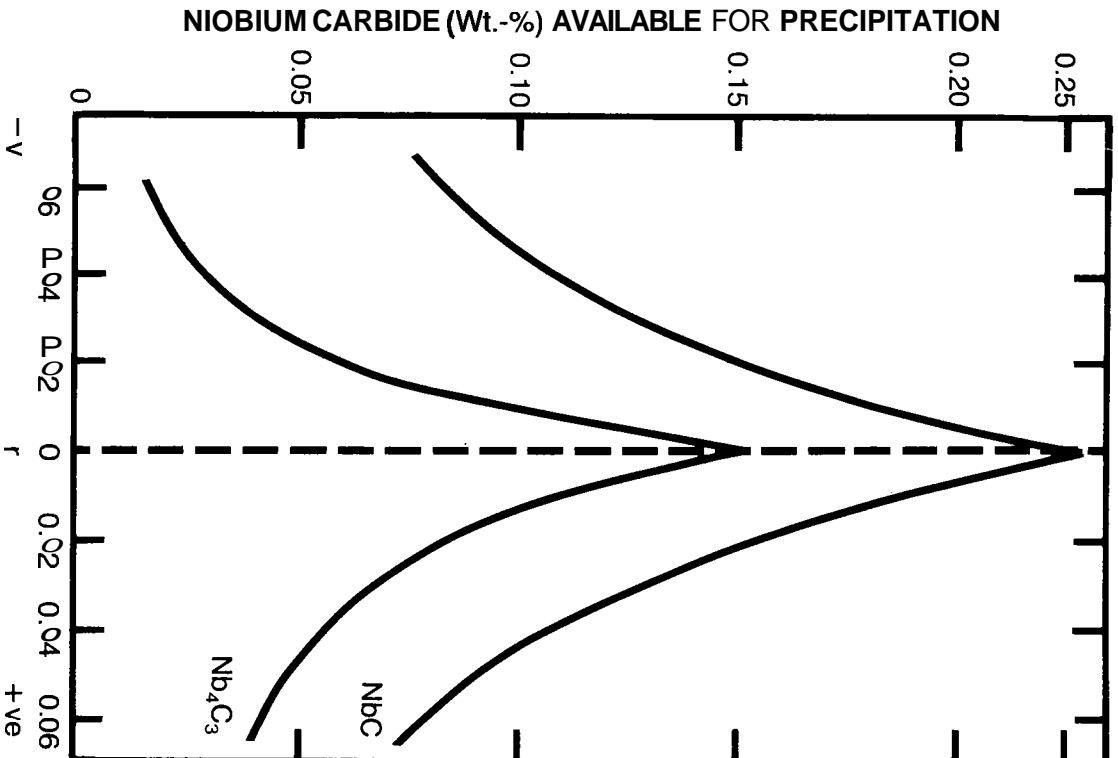


Fig. 2 - Amount of niobium carbide available for precipitation at 923 K (after solution-treatment at 1373 K) as function of degree of deviation from stoichiometry, r. Positive values of r indicate C-rich compositions, negative values Nb-rich. After Wadsworth et al (90).

that the first precipitate to form would be NbN and the precipitation would continue until the Nb in solution in the austenite would fall to .015 Nb. Further precipitation of nitride would occur by formation of NbN and AlN with equal probability.

Solubility products appear to be influenced by the presence of elements which do not directly participate in the precipitate reaction. Koyama, et al., (92) have examined the influence of several elements on the solubility of NbC in austenite. By way of an example, the solubility product for NbC in otherwise unalloyed austenite is about  $5 \times 10^{-3}$  at 1150 C. An addition of Mn increased log K by about 5 percent per percent Mn added, while an addition of Si reduced log K by about 45 percent per percent Si added. The solubility product at 1150 C for a steel that contained 1.5 percent Mn and 0.4 percent Si was  $\approx 4 \times 10^{-3}$ ; the addition of Mn and Si acted to reduce the solubility product by about 20 percent.

Although much work has been done on solubility products, there is still some question as to the overall applicability of these products to typical steels undergoing actual processing. This applicability was tested by Simoneau, et al., (93) and it was shown that a large discrepancy existed between the experimentally determined amount of Nb dissolved in austenite during reheating and the same quantity predicted from several solubility product equations. The comparison of the experimental and theoretical amounts of dissolved Nb is shown in Figure 29; it is clear that there is less than ideal agreement between the experimental and theoretical values due to kinetic and equilibrium considerations. It appears that there is still much work to be done in this general area of solubility products and their applications.

#### Crystallography of Precipitation: Orientation Relationships and Lattice Matching

The crystallography of precipitation in steel has been reviewed recently by Jack and Jack, (94) Davenport, et al. (95) and Honeycombe (96). There are two aspects of the crystallography of precipitation that are of interest in this discussion. These are (a) the orientation relationship that exists between the crystal structure of the precipitate and that of the matrix, and (b) the degree of lattice registry between the precipitate and the matrix.

Carbonitrides of niobium, vanadium and titanium can precipitate in both austenite and ferrite. Several studies (95, 97-99) have shown that when these carbonitrides precipitate in austenitic stainless steel, they do so such that the lattice of the precipitate with the NaCl crystal structure is parallel to the FCC lattice of the parent austenite, i.e.

$$[100]_{M(CN)} \parallel [100]_{\gamma} \quad (9)$$

$$[010]_{M(CN)} \parallel [010]_{\gamma} \quad (10)$$

Davenport, et al., have provided direct evidence that this same relationship holds for the strain-induced precipitation of NbC in austenite in a microalloyed steel (95).

When NbC<sub>x</sub>N<sub>y</sub> precipitates in ferrite (95, 100) or martensite, (101) it does so with the Baker-Nutting orientation relationship: (102)

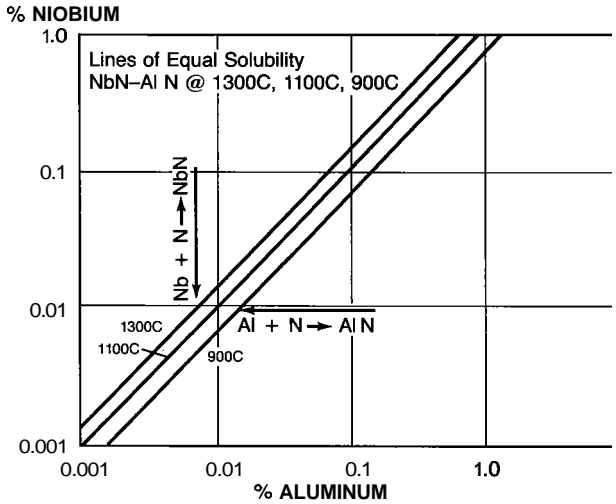


Figure - 28 - Lines of equal solubility for precipitation of AlN and NbN. After Keown and Wilson (91).

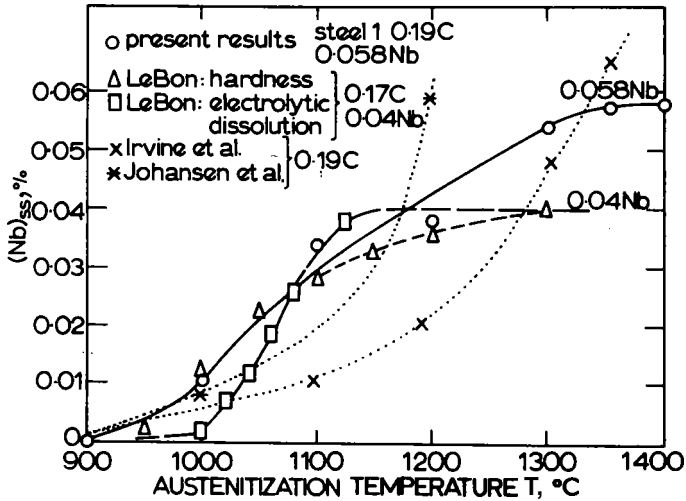


Figure 29 - Influence of austenitization temperature on the amount of Nb in solid solution. Dotted lines are calculated from solubility products. After Simoneau et al (93).

$$[100]_{\text{NbC}} \parallel [100]_{\alpha} \quad (11)$$

$$[011]_{\text{NbC}} \parallel [010]_{\alpha} \quad (12)$$

The "parallel" and Baker-Nutting orientation relationships can be simply illustrated through the use of the appropriate metal-atom octahedra (94). The metal-atom octahedra for austenite,  $\text{NbC}_{\text{x}}\text{N}_{\text{y}}$  and ferrite are shown in Figure 30. The structures of the austenite and  $\text{NbC}_{\text{x}}\text{N}_{\text{y}}$  are positioned to represent the parallel orientation relationship and the structures of the ferrite and  $\text{NbC}_{\text{x}}\text{N}_{\text{y}}$  are positioned to represent the Baker-Nutting orientation relationship. Note that the three octahedra shown in Figure 30 all have a cube plane at the base.

The octahedra shown in Figure 30 also permit the calculation of lattice mismatch. This is done by calculating the percent increase in matrix lattice parameter that would be required to bring the two lattices into coincidence at the matrix-precipitate interface, i.e.,

$$\% \text{ Mismatch} = \frac{L_p - L_m}{L_m} \times 100, \quad (13)$$

where  $L_p$  = appropriate length of octahedron of the precipitate, and  
 $L_m$  = appropriate length of octahedron of the matrix.

Examples of the required distortion or mismatch of the matrix for several types of precipitates are shown in Table IV. The magnitudes of the elastic matrix strains ( $\epsilon = 0.255$  for NbC in austenite and  $\epsilon = 0.105$  and  $0.563$  in ferrite) required for lattice registry would appear to rule out any large degree of coherency between the precipitate and the matrix. However, the elastic strains required of the matrix to achieve lattice registry could be easily accommodated by the presence of a few interfacial dislocations for a precipitate of dimension  $100 \text{ \AA}$ .\*

Table IV. Lattice Mismatch for  $\text{NbC}_{\text{x}}\text{N}_{\text{y}}$  Precipitates in Austenite and Ferrite

Matrix	Orientation Relationship	Required Distortion of Matrix, % <sup>†</sup>		
		NbC	NbC <sub>.8</sub>	NbN <sub>.8</sub>
γ	$[100]_{\text{ppt}} \parallel [100]_{\gamma}$	25.5	26.6	23.0
	$[010]_{\text{ppt}} \parallel [101]_{\gamma}$	25.5	26.6	23.0
	$[001]_{\text{ppt}} \parallel [001]_{\gamma}$	25.5	26.6	23.0
α	$[100]_{\text{ppt}} \parallel [100]_{\alpha}$	56.3	57.7	53.1
	$[011]_{\text{ppt}} \parallel [010]_{\alpha}$	10.5	11.5	8.4
	$[0\bar{1}1]_{\text{ppt}} \parallel [001]_{\alpha}$	10.5	11.5	8.4

<sup>†</sup> All matrix strains are tensile (+).

\* A first-order approximation indicates that about seven and three dislocations would be required to cancel the lattice mismatch for a precipitate of NbC of size  $100 \text{ \AA}$  in austenite and ferrite, respectively.

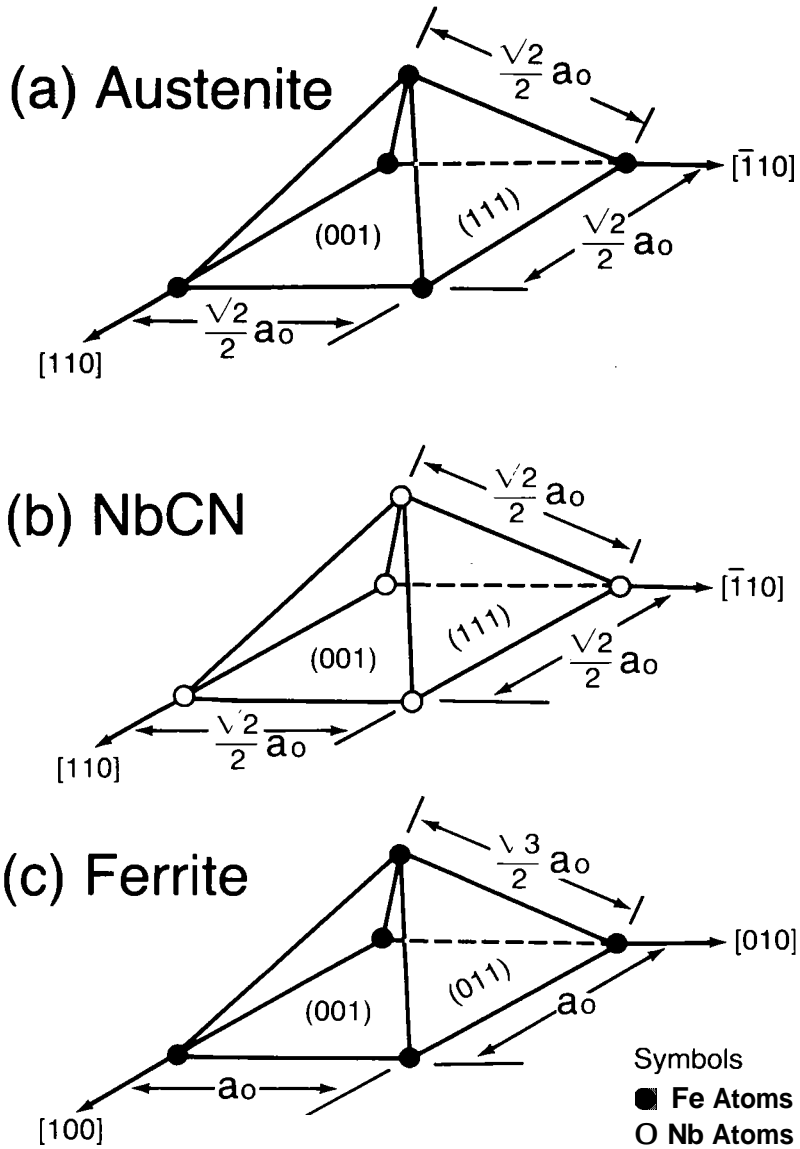


Figure 30 - Metal-atom octahedra for (a) austenite, (b) NbC and (c) ferrite. Adapted from Jack and Jack (94).

The orientation relationship that is observed between the NbC and ferrite can be used to distinguish the NbC which had nucleated in austenite from the NbC which had nucleated in ferrite. As was noted above, NbC forms in austenite with a parallel orientation relationship and in ferrite with the Baker-Nutting orientation relationship. Therefore, all NbC precipitates that show the Baker-Nutting relationship must have formed in the ferrite. The NbC that forms in austenite will not have the Baker-Nutting relationship with the ferrite.

When austenite transforms to ferrite or martensite, it does so with the Kurdjumov-Sachs orientation relationship (103).

$$(111)_\gamma \parallel (110)_\alpha \quad (14)$$

$$[110]_\gamma \parallel [111]_\alpha \quad (15)$$

The consequence of this relationship is that when the matrix transforms from austenite to ferrite, the orientation of the original austenite and the precipitates that formed in that austenite would be related to the ferrite by the Kurdjumov-Sachs relationship. Therefore, the precipitates that formed in the austenite can be identified because they will have the Kurdjumov-Sachs orientation relationship with the ferrite when observed at room temperature. If the orientation of the austenite grains would change after precipitation had occurred, e.g. by grain rotations accompanying deformation or recrystallization, then there would be no rational crystallographic relationship between the NbC that had formed in the austenite and the final ferrite matrix. In principle, this change in austenite grain orientations after precipitation would not appear to be a very frequent occurrence since most of the precipitation that forms in austenite is strain-induced, and these precipitates act to suppress subsequent recrystallization of the deformed austenite in which they formed. However, the coherency (and accompanying stresses) between NbC<sub>x</sub>N<sub>y</sub> and austenite disappear during they → α transformation so that even when there is no further precipitate growth, the ferrite strengthening effect of NbC<sub>x</sub>N<sub>y</sub> formed in austenite is reduced substantially.

#### Precipitation of NbC<sub>x</sub>N<sub>y</sub>: Typical Morphologies and Distributions

The precipitation of NbCN\* in austenite and ferrite is heterogeneous in nature, i.e. it always occurs in conjunction with crystalline defects such as grain boundaries, incoherent twin boundaries, stacking fault boundaries and subgrain boundaries. One reason why the precipitation forms in this fashion is the rather large mismatch between the lattice of NbCN and the matrix, austenite (54, 63, 71-75) or ferrite (53, 63, 69, 74, 76-82) Table IV. These crystalline defects are sources of dislocations which can act to cancel some of the elastic strain which may develop during the formation of the precipitates.

---

\* Hereinafter, NbCN will be used to denote NbC<sub>x</sub>N<sub>y</sub>.

In one of the few studies that have been done on the precipitation of NbCN in recrystallized austenite, Santella has shown that the NbCN forms almost exclusively on grain boundaries, (69) as is the case for precipitation in casting (80). Much more research has been done on NbCN precipitation which has formed in deformed austenite and in ferrite. Good illustrations of strain-induced precipitates of NbCN in deformed austenite are available in the literature, (15, 95, 104-107) and an example is presented in Figure 31. In every case, the precipitates appear to decorate what was once a grain or subgrain boundary in the prior-austenite.

When NbCN precipitates in ferrite, the nature of the precipitate distribution is related to the nature of the austenite-to-ferrite transformation. If the ferrite which forms has a polygonal morphology, the NbCN precipitation will have the "interphase" distribution (40, 96). During the interphase precipitation, the NbCN forms along the advancing austenite-ferrite phase boundary. When the boundary moves to a new location, the precipitates are left behind in a sheet-like array. The final microstructure consists of numerous sheets of precipitates, where each sheet denotes the location of the interphase boundary during the course of the transformation. This form of precipitation in Nb steels has been observed by Gray and Yeo (40) and others (95, 108, 109) and an example is given in Figure 32.

When precipitation occurs substantially after transformation is complete, such as during slow cooling after low-temperature coiling on a strip mill, the precipitate has a more uniform distribution (40). These precipitates and associated strain fields are responsible for the strong precipitation hardening effect of NbCN.

Similar distributions occur in ferrite which has an acicular or bainitic character (95). Furthermore, there is great similarity in distributions and morphologies between the NbCN that forms in acicular ferrite and the NbCN that forms during secondary hardening in the tempering of a quenched steel (101). An example of this general type of precipitation of NbCN in a is given in Figure 33.

The strengthening effect of these precipitate distributions is considered to result from looping of dislocations between the more widely spaced particles. The most generally accepted theory which described particle looping is that of Orowan, (110) modified by Ashby, (111) and by Gladman, et al., (34) who developed the Orowan/Ashby model to give the effects of precipitate size and volume fraction. Despite the complexity of their derivation, the result can be presented in simple form as shown in Figure 34, (34). Although deviations from the model have been observed, (73) the approach still allows one to estimate expected strengthening increments for most steels as illustrated in Figure 35, (73).

#### Kinetics of Precipitation of NbCN in Austenite

The response of a steel to a given thermal and deformation history is closely related to the kinetics of dissolution and of reprecipitation of NbCN in austenite. While the best publicized thermomechanical treatment is "controlled rolling" of plate and pipe steels, there are several other metallurgical objectives that can be achieved by proper balance of the deformation recovery-precipitation interactions. Some of these are listed below for completeness.



Figure 31 - Strain-induced precipitation of NbCN in austenite in a steel containing .09 percent C - .07 percent Nb. Specimen reheated at 1250 C, rolled 25 percent and held at 950 C, and air cooled to RT. Centered dark field electron micrograph using a (111) NbC reflection. After Santella (69).

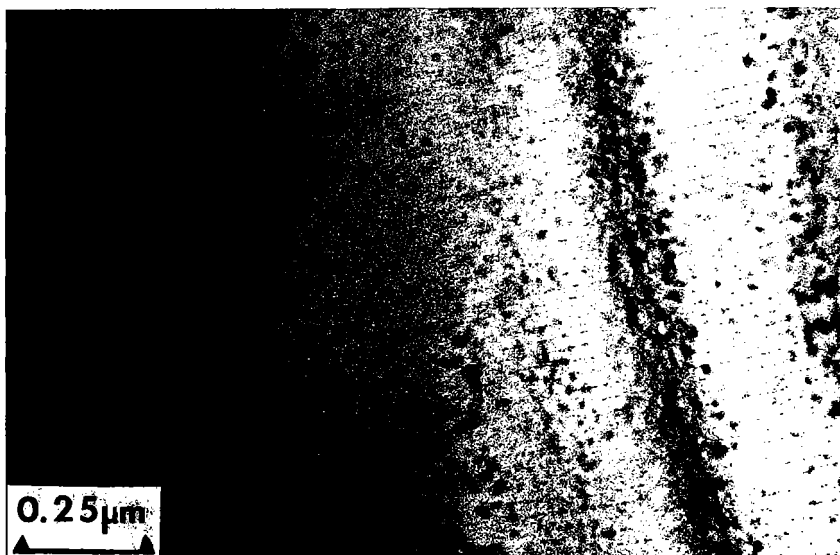


Figure 32 - Interphase precipitation of NbCN in ferrite in steel containing .09 percent C - 0.7 percent Nb. Specimen was reheated to 1250 C, hot rolled to 1000 C and air cooled to RT. Bright field electron micrograph. After Santella (69).

0.25  $\mu\text{m}$

Figure 33 - General precipitation of NbCN in ferrite in steel containing .09 percent C - .07 percent Nb. Specimen reheated to 1250 C, hot rolled to 1000 C and air cooled to RT. Dark field electron micrograph using a  $\langle 111 \rangle$  NbC reflection. After Santella (69)

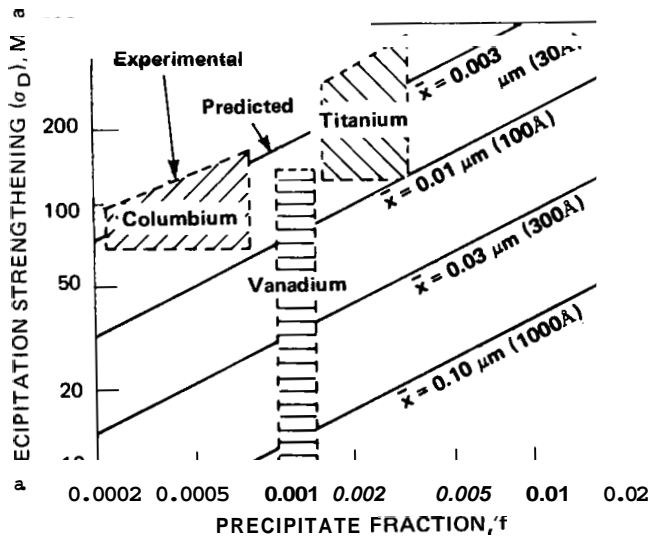


Figure 34 - The dependence of precipitation strengthening on precipitate size ( $\bar{x}$ ) and fraction according to the Ashby-Orowan Model, compared with experimental observations for given microalloying additions. After Gladman, et al (34).

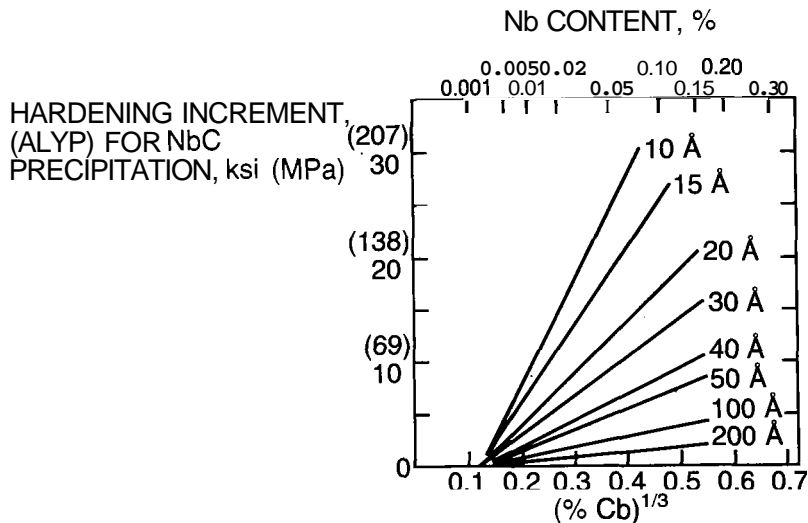


Figure 35 - Effect of precipitate volume fraction and particle size on yield-strength increment. After Gray (73).

a. For sheet and strip, if one is interested in high strength, then it is appropriate to maximize soluble niobium at the time of the  $\gamma \rightarrow \alpha$  transformation.

b. For cold-rolled steel, it may be desirable to try to develop a specific hot-band texture for inheritance by the ferrite after transformation. As referenced earlier, the sharpness of the texture is affected by the retardation of recrystallization by niobium and increases with cooling rate and reduction in finish rolling and transformation temperature (37).

c. It may be appropriate to produce a specific precipitate distribution or to control the grain growth during conventional heat treatments (44, 45) or to aid in the development and/or selection of appropriate texture during annealing after cold rolling (39).

d. For some applications, it is desirable to develop continuous-yielding stress-strain curves. In such cases one may process to engineer a specific transformation behavior by virtue of interaction between segregation, banding tendencies and finishing rolling temperature. In addition to changes in yielding behavior it may be possible to change HIC resistances of microalloyed steels during thermomechanical manipulation.

e. It may be possible to remove undesirable interstitials from solid solution by strain-induced precipitation at high temperatures. For example, formation of nitrogen-rich NbCN might preempt reaction of nitrogen with boron or aluminum at lower temperatures.

In a broad sense, all of these objectives might be covered under the banner of "controlled rolling" or austenite conditioning.

When a Nb-bearing low-alloy steel is in the austenite phase field, the Nb will be in both the solid solution matrix and in the precipitated NbCN. At equilibrium, this partitioning of Nb between the matrix and precipitate will be controlled by the solubility relations discussed earlier. Since one of the primary requisites of a successfully conditioned austenite is the presence of a large number of crystalline defects that can act as sites for ferrite nucleation during cooling, the motion of subgrain and grain boundaries associated with static recrystallization and grain growth after hot deformation must be retarded. Evidence for this retardation by Nb in both solid solution (112-114) and in precipitate (115-117) can be found in the literature.

The different effects of NbCN precipitation during hot rolling have stimulated a large number of studies concerned with the kinetics of precipitation in austenite as influenced by composition, strain, strain-rate, temperature and overall heat treatment. This group of studies of precipitation kinetics has utilized a wide variety of techniques including: chemical analysis, (56, 66, 68, 83, 112, 118) electrical resistivity, (93, 119) X-ray diffraction, (105) quantitative electron microscopy, (107) flow curves (114) and hardness testing, (29, 112, 120). The precipitation which has been studied in these experiments is, with one exception, the strain-induced precipitation which occurs during and/or after deformation. The exception is the dynamic precipitation which accompanies deformation and which has been studied by Jonas, et al., (114, 121).

Studies of the precipitation in recrystallized austenite have shown that the kinetics are very sluggish (65, 93, 119). The results of the study by Simoneau, et al., (93) on precipitation rates at temperatures above 900 C are shown in Figure 36. The kinetics of NbCN precipitation at 900 C are shown in Figure 37; these data are from the work of LeBon, et al. (112). Finally, the precipitation kinetics at low temperatures, below 950 C, have also been determined by Watanabe, et al.; (65) these results are shown in Figure 38. These studies illustrate the slow rate of precipitation in recrystallized austenite; it takes several thousands of seconds at 900 C for 50 percent of the potential precipitation to form. Also, by combining the results of Simoneau, et al., (93) and Watanabe, et al., (65) the overall precipitation behavior **does** appear to conform to C-curve kinetics.

The precipitation rate is remarkably sensitive to the level of strain imparted prior to aging, as is illustrated by the results of LeBon, et al., (112) Figure 38, and Hoogendorn and Spanraft, (118) Figure 39. The strain-induced precipitation of NbCN in austenite appears to follow C-curve kinetics, with the nose of the curve located between 900 and 950 C. Three C-curves, each based on a different technique, are shown in Figures 39, 40 and 41. These results are from the work of Watanabe, et al., (65) Figure 38; Ouchi, et al., (29) Figure 40; and Hansen, et al., (107) Figure 41. In all three cases, the nose of the C-curve appears to be in the temperature range 900 to 950 C.

The overall composition of the steel appears to have a strong effect on the kinetics of precipitation (65, 114, 120). For example, the presence of Mo appears to shift the C-curve to lower temperatures and shorter times, (65) whereas an increase in Mn level acts to shift the C-curve to longer times (121).

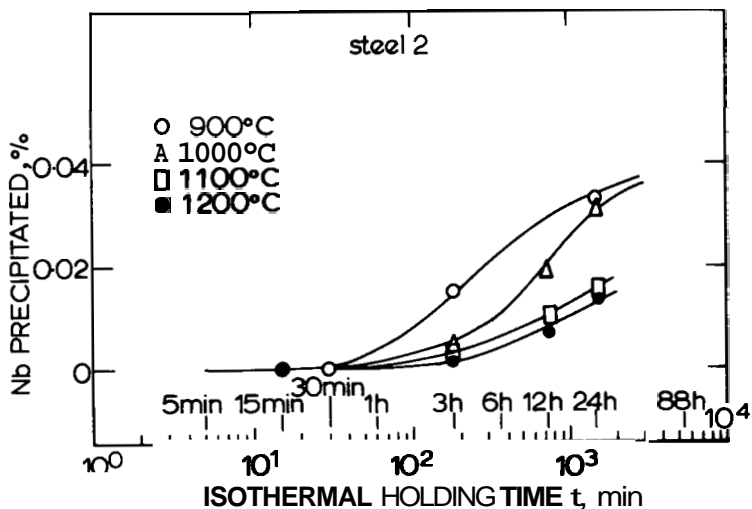


Figure 36 - Isothermal precipitation of Nb in undeformed austenite in steel containing .07 percent C - .04 percent Nb - .010 percent N. After Simoneau (93).

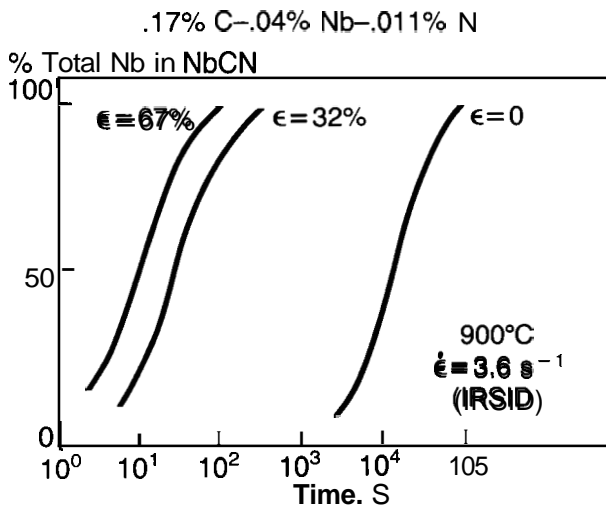


Figure 37 - Influence of strain level on the kinetics of Nb precipitation at 900 C. After Lebon and Saint-Martin (14).

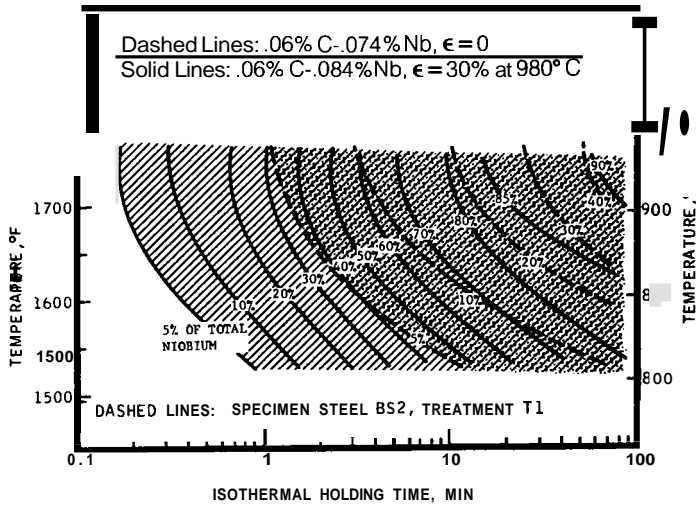


Figure 38 - Time-temperature-precipitation diagram showing effect of deformation on precipitation on Nb (C,N) in Austenite. After Watanabe et al (65).

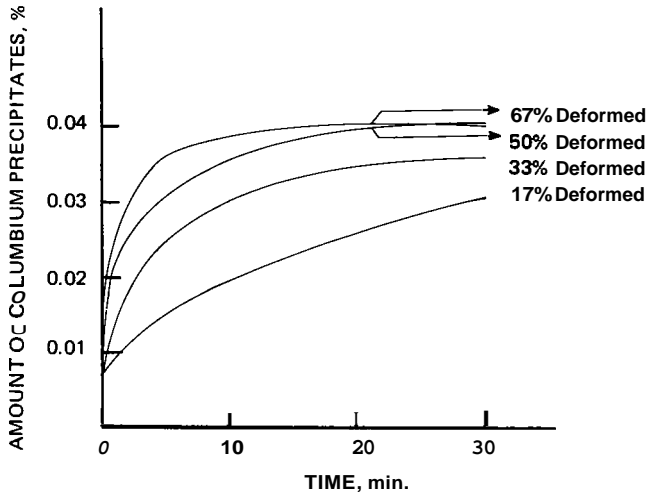


Figure 39 - Influence of deformation and precipitation in a steel containing 0.06 percent carbon, 0.041 percent columbium, and 0.0040 percent nitrogen. After Hoogendorn and Spanraft (118).

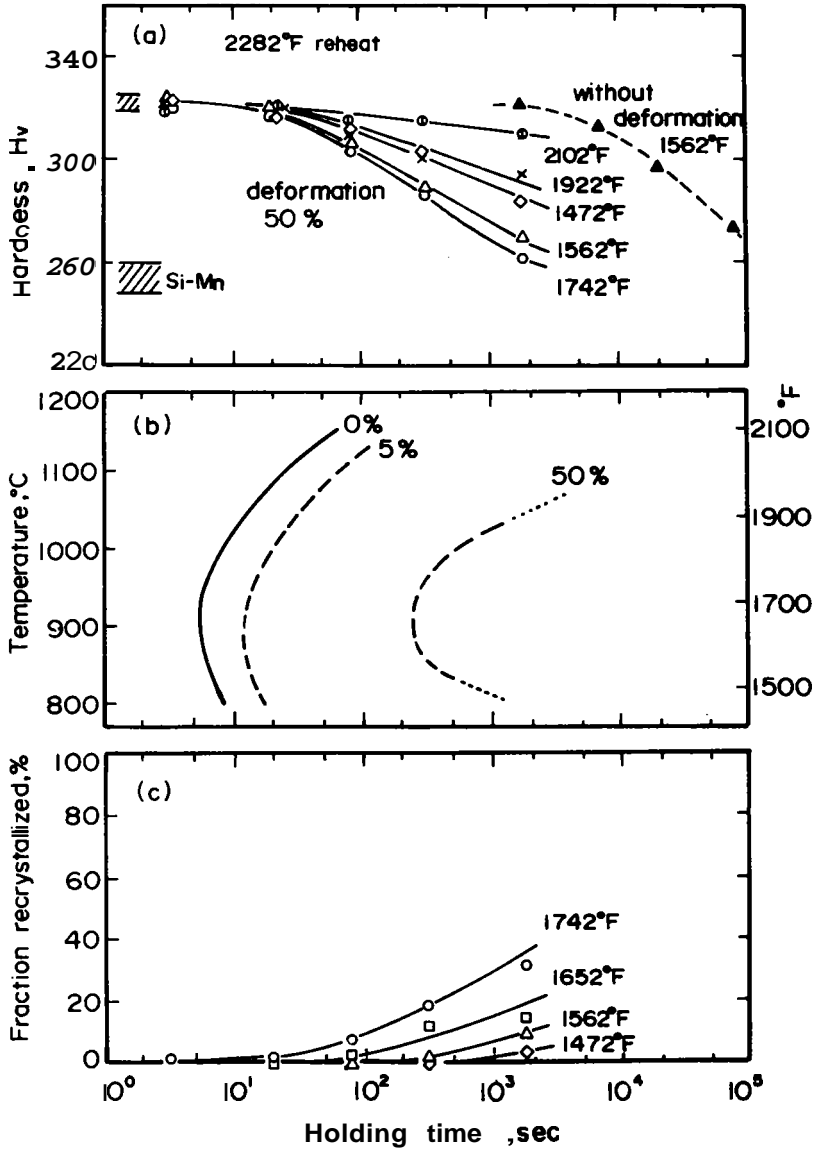


Figure 40 - Precipitation of Nb (CN) and recrystallization kinetics during isothermal holding in Nb-bearing steel, (a) hardness changes after tempering at 1112 F (600 C), (b) precipitation kinetics and (c) recrystallization progress. After Ouchi et al (29).

Studies of the precipitation of NbCN in deformed austenite are subject to certain problems when the temperature of deformation (and subsequent holding) are raised. The problem arises because the density of crystalline defects in the austenite does not vary continuously with temperature over a large temperature range, say,  $800 < T \leq 1200$  C. For a given set of conditions of composition, temperature, strain and strain-rate, the austenite deformed at high temperatures may experience recrystallization. This would be expected at large strains, high temperatures and low strain rates. The austenite deformed at **low** temperatures will be highly elongated and the austenite deformed at intermediate temperatures will have a mixed equiaxed plus elongated grain structure. Behavior of this kind would be expected to give a discontinuous relationship between the crystalline defect density that can act as nucleating sites for NbCN precipitation and the deformation temperature. This type of austenite deformation behavior has been observed in microalloyed steels (86, 105) and has been shown to influence the results of precipitation kinetic studies (105). An example of this effect is shown in Figure 42, which has been taken from the work of Davenport, et al. (105) Figure 42, where the relative integrated intensity is assumed to be roughly proportional to the volume fraction of precipitate, indicates that there are high rates of precipitation in the temperature range 950 to 1100 C and lower rates at temperatures which are either above or below this range. Davenport, et al., (105) have noted that the lowering of precipitation kinetics which results from higher temperature deformation and holding may be due to two effects. The first is the reduction in solute supersaturation with increasing temperature; this alone would lead to a decrease in precipitation rate. The second is the change in deformation structure of the austenite near 1100 C. Austenite rolled below this temperature leaves the rolls with an elongated, deformed microstructure which contains numerous sites for strain-induced precipitation. Austenite rolled above this temperature leaves the rolls in the dynamically recrystallized state; this structure contains few sites for strain-induced precipitation; hence, low precipitation kinetics can be expected.

The studies of precipitation kinetics described to this point have involved "static" precipitation. That is, the austenite has been deformed in one operation and then aged in a second operation. A different approach to studying strain-induced precipitation has recently been developed by Jonas, et al. (114, 121). This approach enables the kinetics of strain-induced precipitates to be determined in a "dynamic" context, i.e. where the austenite is being strained and aged at the same time. This approach yields C-curves describing the dynamic precipitation and is based on the analysis of hot flow curves. C-curves describing this dynamic precipitation (121) are shown in Figure 43.

The kinetics of the precipitation of NbCN in austenite have been summarized and are presented in Table V and Figure 44. Figure 44 shows the time required for 50 percent of the precipitation of NbCN to be completed as a function of the amount of strain experienced by the austenite in the temperature range of 900-950 C. The marked influence of strain level on the kinetics of precipitation is clear; the kinetics increase rapidly with increased strain. For example, whereas it might take 500 to 800 seconds for 50 percent of the precipitate to form after small strains ( $\leq 15\%$ ), it would take only 30 to 40 seconds after longer strains ( $50 < \epsilon \leq 60\%$ ), Figure 44. While the trend in this compilation is distinct, there is considerable scatter which is not unexpected due to the differences in base chemical composition, strain rate, testing technique (method of straining), solution treatment condition and other relevant factors.

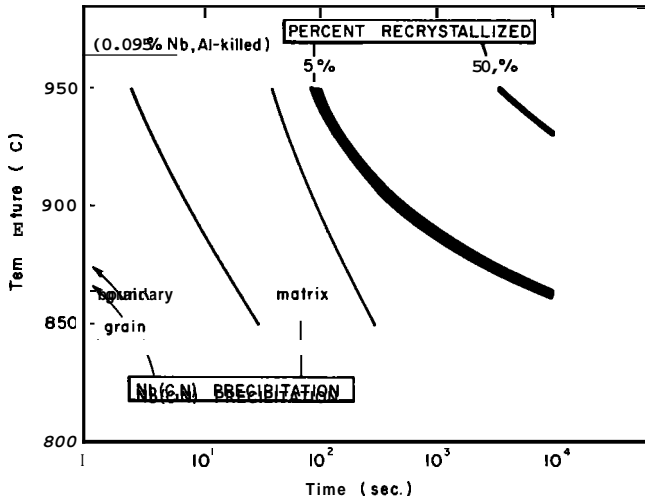


Figure 41 - Recrystallization/precipitation/temperature/time (RPT) diagram for steel 3 after solutionizing at 1250 C and hot rolling 50 pct at 950 C. After Hansen et al (107).

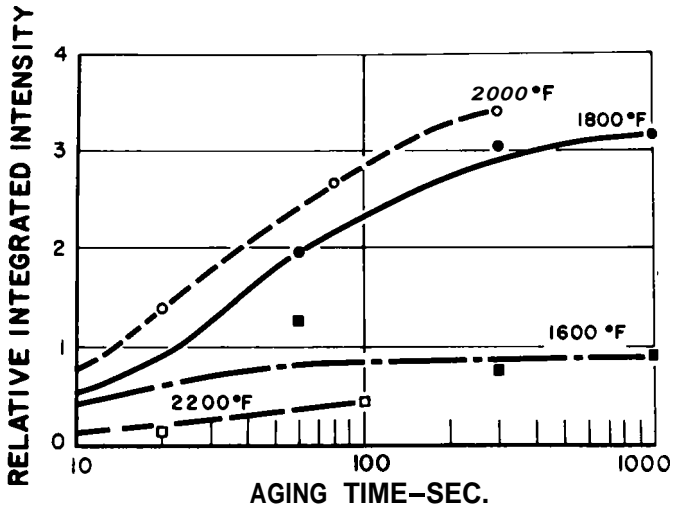


Figure 42 - Relative integrated intensity versus aging time for samples deformed 60 percent at the indicated temperatures. After Davenport et al (105).

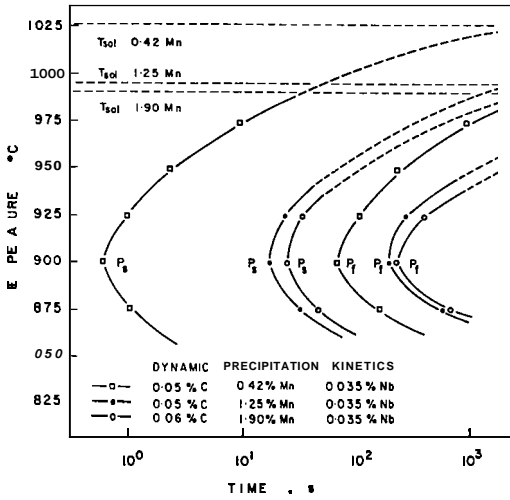


Figure 43 - PTT curves for dynamic precipitation of NbCN in austenite. After Akben et al (121).

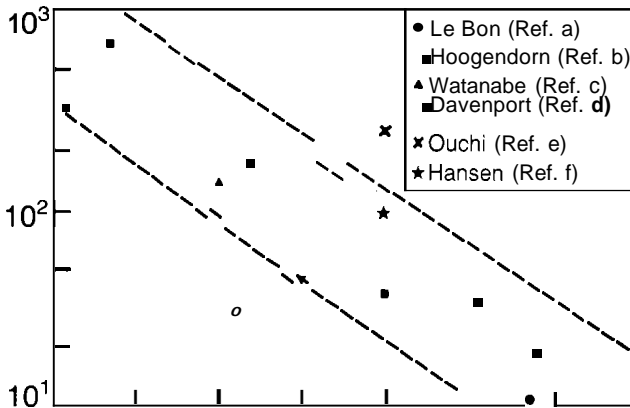


Figure 44 - Compilation of kinetic data for the strain-induced precipitation of NbCN in austenite. Ref. a=14, b=118, c=65, d=105, e=29 and f=107.

Table V. Summary of Observed Kinetics of NbCN Precipitation in Austenite

% Nb In Steel	Hot Deformation	Analytical Method	Conditions for 50% Pptn.		Ref.
			Strain, %	Time, secs.	
.04	Torsion at 900°C	Chem. Ext.	0	14.6 x 10 <sup>3</sup>	112
			32	31	
			67	11	
.04	Rolling at 900°C	Chem. Ext.	17	678	118
			33	174	
			50	38	
			67	19	
.08	Rolling at 925°C	Chem. Ext.	0	6 x 10 <sup>3</sup>	65
.09	Rolling at 982°C	Semi-Quan, X-ray	40	48	105
			60	36	
.04	None at 900°C	Elect. Resistivity	0	16.8 x 10 <sup>3</sup>	93
.031	Rolling at 900°C	Hardness	50	253	29
.035	Compression at 900°C	Strength	*	65	114
.03	Held at 950°C	Quantitative	50	100	107

One of the principal reasons why the precipitation studies discussed above were performed was to assess the way in which the precipitation of NbCN would occur and, hence, the way in which this precipitation could interfere with the recovery and recrystallization of the deformed austenite. It would be instructive, therefore, to briefly analyze what kind of information would be determined in each type of precipitation study (i.e. technique), relative to the information which is required to evaluate the potential retardation of static recovery and recrystallization.

It has been shown (122) that an array of spherical particles can apply a force per unit area on a boundary moving during primary static recrystallization

$$\frac{F_{\text{retard}}}{\text{Area}} = \sigma_{\text{retard}} = \frac{3f\gamma}{2R} \quad (16)$$

where  $f$  is the volume fraction,  $\gamma$  is the boundary surface energy and  $R$  is the particle radius. Furthermore, it has been shown by Gladman (34) that the geometrical characteristics of a precipitate dispersion of the type found in microalloyed steels can be given by

$$L = D \sqrt{\frac{\pi}{4f}} \quad (17)$$

where  $L$  is the average interparticle distance and  $D$  is the average particle diameter. This relationship among the precipitation dispersion parameters is shown in Figure 45, along with values typically found in Nb steels.

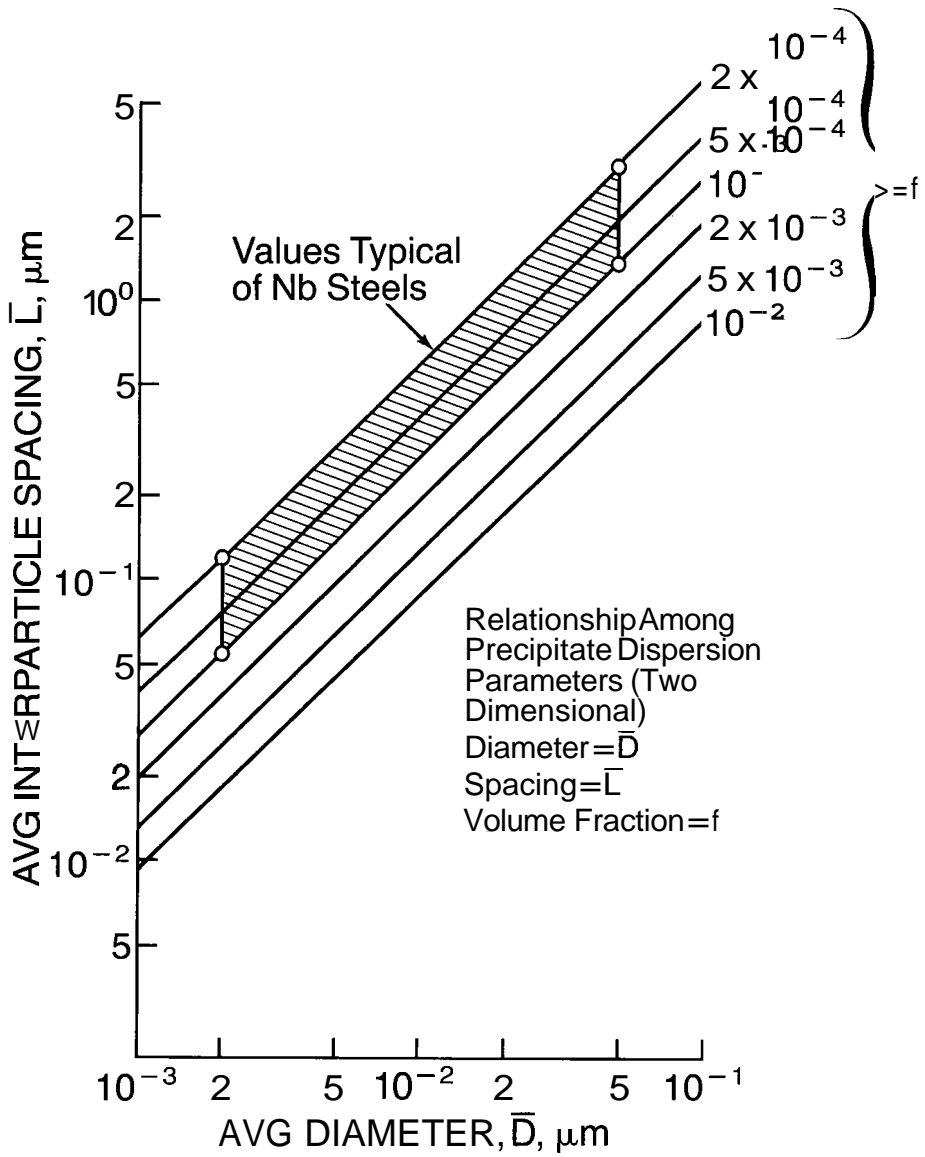


Figure 45 - Relationship among precipitate dispersion parameters: diameter ( $\bar{D}$ ), spacing ( $\bar{L}$ ) and volume fraction ( $f$ ).

Taken together, these two equations mean that the correct assessment of the magnitude of the stress acting to retard recrystallization can only be made if two of the three precipitate dispersion characteristics ( $f$ ,  $R$  and  $L$ ) are known. Hence, the retarding stress can be expressed as

$$\text{retard } \sigma = k_1 \frac{\sigma}{R} = k_2 \frac{\sigma}{L} = k_3 \frac{\sigma}{f} \quad (18)$$

where  $k_1$ ,  $k_2$ ,  $k_3$  are numerical constants which include the surface energy term.

At this point, it is possible to evaluate how the results of the various precipitation studies can be interpreted relative to a  $\sigma_{\text{retard}}$ . The studies that utilize the chemical analysis of extracted particles (56, 65, 68, 112, 118) provide information concerning  $f$  alone. This is also true for the studies that involved electrical resistivity, (93, 119). The precipitation studies of Davenport, et al., (105) which involved X-ray and TEM analyses, and those of Hansen, et al., (107) which involved quantitative TEM, included efforts to evaluate both  $f$  and  $R$  for several NbCN precipitate dispersions in rolled and aged steels. These data should permit the calculation of  $\sigma_{\text{retard}}$  as well as its temperature dependence. However, the kinetics of static recrystallization in both of these studies clearly indicate that all of the precipitation which occurs below about 950 C is quite capable of severely retarding static recrystallization and, hence, this precipitation must generate relatively large retarding stresses.

#### Influence of Niobium on the Response of Austenite to Thermomechanical Treatment

Many of the benefits that are observed when Nb is added to steel occur because the Nb can alter the response of austenite to reheating, hot deformation and recrystallization.

Several studies have been conducted on the influence of Nb on the grain coarsening behavior of austenite during reheating, (24-27, 29, 113, 123). These studies have shown that Nb can drastically alter the grain size of reheated austenite, especially at low austenitizing temperatures, i.e. below about 1150 C.

When grains undergo grain growth, they do so because this enables the average grain boundary curvature to be increased and the total surface energy of the system to be decreased. Under the conditions where there is no large barrier to boundary migration, i.e. by solute atoms, particles or free surfaces, the boundaries can move in a relatively unhindered fashion and the grains will coarsen in a monotonic way with time and temperature. This process is termed "normal" grain coarsening and is characterized by a single distribution of grain diameters, the average of which will increase with time and temperature, (124, 126).

If normal grain growth is suppressed by the presence of solute atoms, particles, free surfaces or textures, but additional thermal activation is supplied which enables these barriers to be overcome, then exaggerated growth of a few select grains can occur. This is called "abnormal" grain growth or secondary recrystallization, (127, 128). During abnormal grain growth, the small, primary grains are consumed by the large abnormal grains, and the

process continues until the small, primary grains are replaced by the large, abnormal grains. Before abnormal grain growth begins, the material is composed of primary grains. During abnormal grain growth, the specimen would contain both the small, primary and large, abnormal grains. Upon completion of the abnormal grain growth, the specimen would contain only the large, abnormal grains. The growth of these large grains would then proceed by normal grain growth.

Austenite grains which are coarsening by normal grain growth would follow the normal grain coarsening law (124, 126)

$$D^2 - D_0^2 = k_0 t \exp (-Q/RT) \quad (19)$$

where  $D$  and  $D_0$  are the average grain sizes at times  $t$  and  $t = 0$ , respectively;  $k$  is a constant,  $t$  is the coarsening time,  $Q$  is the apparent activation energy with a value near 18 kcal/mole<sup>°K</sup> (113) and  $R$  and  $T$  have their usual meanings. This type of coarsening behavior will result in a straight line when the log of the grain diameter\* is plotted against either the reciprocal temperature or the log of time. Conversely, when the grain coarsening takes place by abnormal grain growth, the coarsening data will not conform to the normal grain coarsening law, and the data will deviate from the straight lines discussed above. Both types of grain coarsening behavior have been found for the austenite in a C-Mn-Si steel, as illustrated in Figure 46 (26). The steel, in Figure 46, exhibited normal grain growth at temperatures above 1100 C, and the abnormal coarsening after long times at 900 C and short times at 1000 C. When .07 wt percent Nb is added to the C-Mn-Si steel, the grain coarsening behavior changes, as is shown in Figure 47 (26). In this case, the austenite exhibits normal coarsening at temperatures above 1200 C and abnormal coarsening at lower temperatures. The abnormal grain growth exhibited in Figure 47 was a direct result of NbCN precipitation which suppressed the normal grain growth at low temperatures, and which permitted abnormal grain growth to occur as the particles themselves coarsened and dissolved at the higher temperatures.

A different and possibly more useful way of displaying grain coarsening data is with isochronal diagrams of the type shown in Figure 48 (26). The austenite in the base steel, A1, has a rather large grain size at 950 C and does not coarsen very appreciably with temperature. The Nb-bearing steel, A3, has a very fine grain size which does not coarsen with temperature until the onset of abnormal grain growth at 1050 C. The abnormal grain growth is completed at 1200 C, after which the grain size increases very strongly with temperature. The third steel, steel A7, contains both Nb and high nitrogen; the abnormal grain growth is just barely completed at 1250 C in this steel. Electron microscopy has revealed that the absence of normal grain growth of the primary austenite grains at temperatures < 1050 C is caused by the presence of fine NbCN. These precipitates effectively pin the grain boundaries thereby causing the lack of grain growth. As the temperature is increased, however, the particles coarsen and dissolve, and at temperatures above 1050 C they can no longer keep the boundaries from moving. Abnormal

---

\*  $D_0$  is usually neglected in the application of this equation since it is often very much smaller than  $D$ .

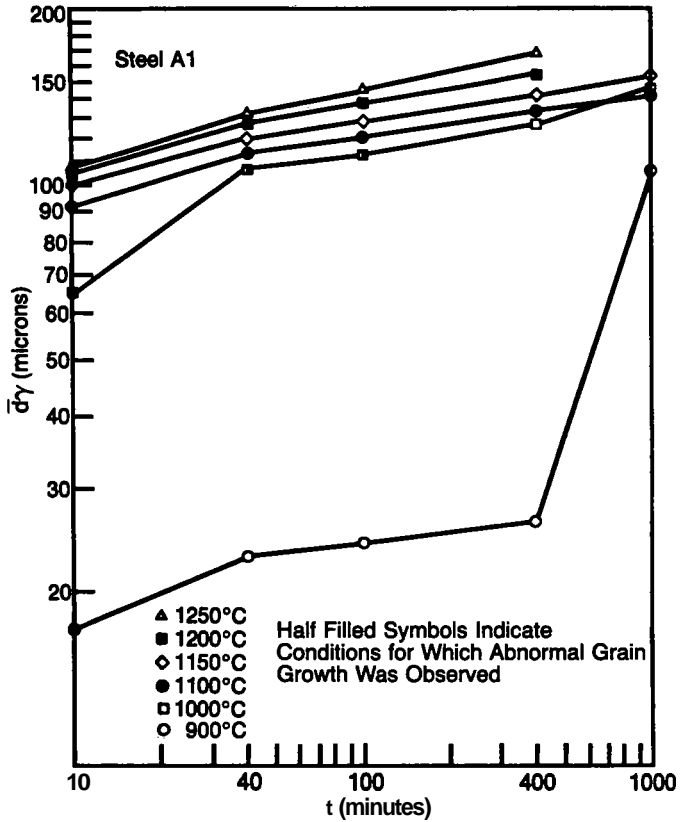


Figure 46 - Isothermal grain coarsening behavior of austenite in steel containing .09 percent C - 1.0 percent Mn - .006 percent N. After Santella (69).

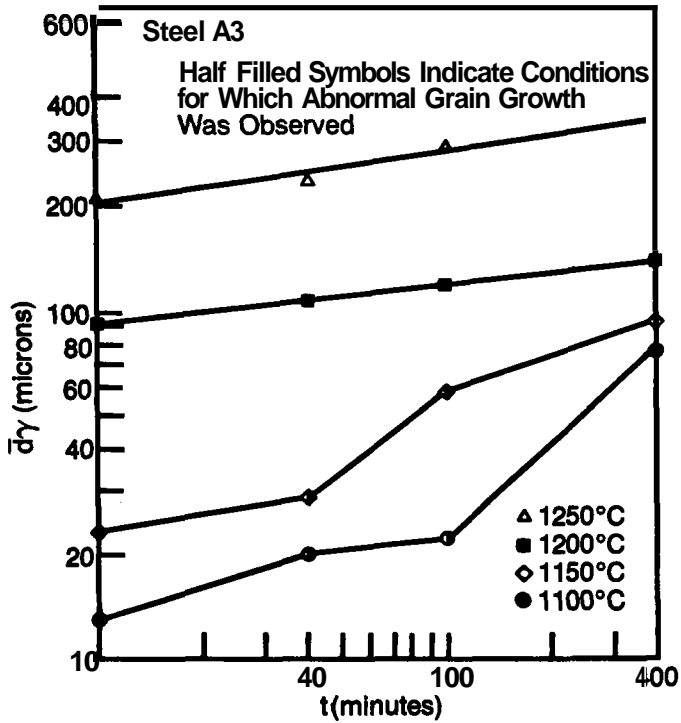


Figure 47 - Isothermal grain coarsening behavior of austenite in steel containing .09 percent C - 1 percent Mn - .07 percent Nb - .006 percent N. After Santella (69).

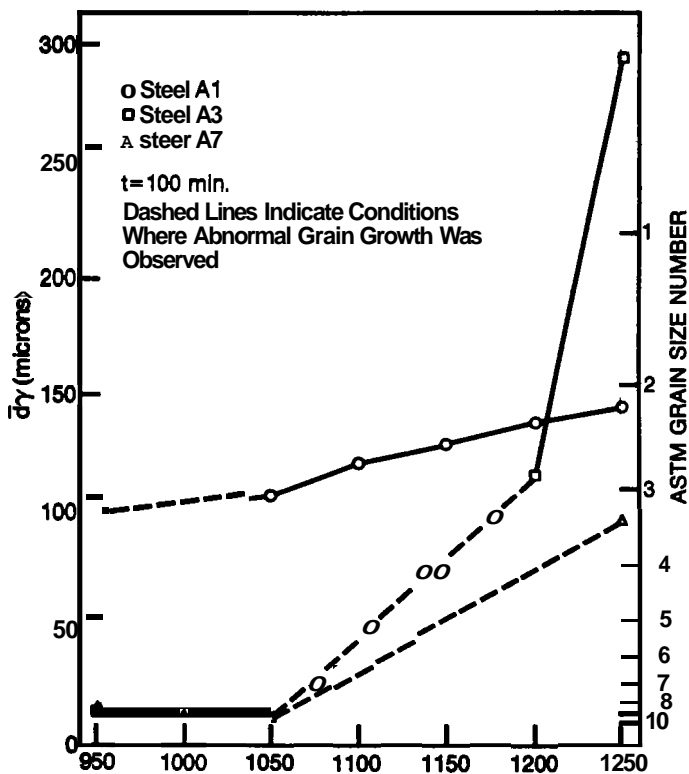


Figure 48 - Isochronal grain coarsening behavior of austenite. Steels A1 and A3 as described in Figures 46 and 47. Steel A7 contains .09 percent C - 1 percent Mn - .07 percent Nb - .023 percent N. After Santella (69).

grain growth can then commence and continue until the fine primary grains are completely consumed. The difference in coarsening behavior between steels A3 and A7 is a result of the presence of a second array of precipitates in A7, one in addition to the fine NbCN found at low temperatures,  $\leq 1050$  C. This second array is a very stable, nitrogen-rich NbCN which remains undissolved up to 1250 C (26). It is this precipitate which keeps the abnormal grain growth stage from being completed below 1250 C.

The grain coarsening behavior of austenite in a Nb steel, therefore, consists of three stages. The first stage occurs at low temperatures, generally below 1000/1050 C, and is associated with very little sensible grain growth. The second stage commences with the initiation of secondary recrystallization and continues until the entire set of primary austenite grains is consumed by the secondary grains. The third stage, which typically starts at 1150/1200 C, consists of the normal growth of the secondary grains, i.e., the grains that resulted from the completion of the secondary recrystallization of the primary grains. During stages two and three, the average grain size of the austenite increases very rapidly.

The conditions which prevail at the point where the particles can no longer effectively pin the grain boundaries, i.e., the end of stage one coarsening, have been discussed by Gladman and Pickering (129). They have shown that the critical (maximum) particle size,  $r_{crit}$ , that can effectively pin the boundaries of austenite of average size  $\bar{R}$  can be expressed as

$$r_{crit} = \frac{6\bar{R}_0 f}{\pi} \left( \frac{3}{2} - \frac{2}{z} \right)^{-1} \quad (20)$$

where  $f$  is the volume fraction of particles and  $z$  is the inhomogeneity factor, the ratio of the radii of the growing grain and the matrix grains. When the particle size exceeds  $r_{crit}$ , the primary austenite grains will no longer be pinned and grain coarsening by secondary recrystallization will begin.

The addition of Nb to a low-carbon steel results in drastic changes in the flow curves during hot deformation (114, 121, 130-134). Since the hot flow curve is sensitive to the dynamic balance which is achieved between work hardening, dynamic recovery, dynamic recrystallization and dynamic precipitation, (114, 121, 135, 136) it is clear that the Nb has substantially altered the hot deformation behavior of the austenite. In general, the addition of Nb causes an increase in the flow stress, an increase in the strain to maximum stress and an increase in the critical strain for the onset of dynamic recovery and recrystallization, (114, 121, 131-134). A good example of this effect is shown in Figure 49 (133). The observation that Nb increases the critical strains for dynamic recovery and recrystallization is an important one. Since the peak and critical strains decrease with increasing deformation temperature, (133, 134) one of the influences of Nb can be considered to be to shift the temperature where dynamic recrystallization could occur to higher temperatures, for a given total strain and strain rate. In other words, the addition of Nb would be to increase what is called the recrystallization temperature for a given strain and strain rate. This influence of Nb on the recrystallization temperature of austenite has, in fact, been observed in several studies of hot rolling where specimens were given reductions of constant strain and strain rate. For example, the so-called recrystallization temperature for C-Mn and C-Mn-Si steels is generally in the temperature range 850-950 C for single pass reductions of 40 to 50

percent on laboratory rolling mills which roll at strain rates in the range 1 to 5 sec<sup>-1</sup> (29, 86, 135). When Nb-bearing steels are subjected to equivalent rolling reductions, the recrystallization temperatures are normally in the range 1050-1150 C, (26, 29, 105, 136). The addition of Nb has been responsible for increasing the recrystallization temperature by about 200 C, (137, 138). A similar effect has been found by Cuddy (139) during the hot compression testing of Nb steels, Figure 50.

Another important role played by Nb is to inhibit the static recrystallization of the deformed austenite which might occur after the deformation is completed. The static recrystallization which can follow hot deformation has been the subject of several investigations in recent years, (24, 29, 105, 107, 112, 113, 118, 130, 132, 133, 137-142). The recent work by Luton, et al. (132) is particularly interesting and important. This study illustrates the fact that Nb suppresses static recovery and recrystallization and also indicates that both the Nb in solution and NbCN particles play important roles in these events. A typical set of results taken from the study of Luton, et al., (132) is shown in Figure 51. The data illustrate the static softening behavior of the base steel (C) and Nb-bearing steels with normal (A) and with very low (B) interstitial levels. The experiment consisted of running hot compression tests at, in this case, 900 C and at a strain rate of 10<sup>-1</sup> sec<sup>-1</sup>. The tests were interrupted after strains of 0.10, and the specimens were unloaded and held at 900 C for various times after which they were once again deformed. The extent of softening (fractional softening) was then calculated from the two flow curves by the use of the following equation.

$$X = \frac{(\sigma_0 - \sigma_2)}{(\sigma_0 - \sigma_1)} \quad (21)$$

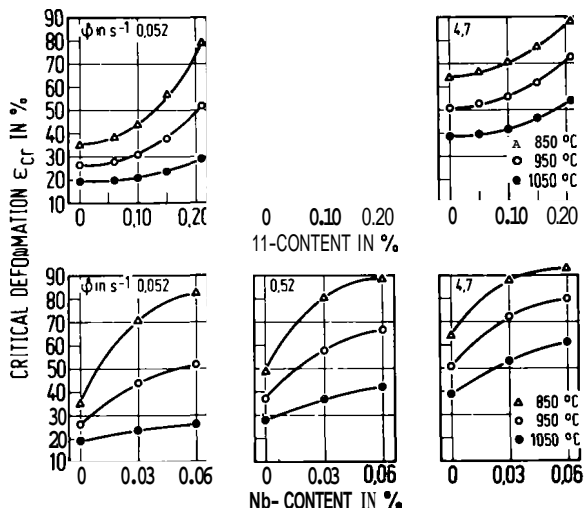


Figure 49 - Influence of Ti and Nb on the deformation required for dynamic softening in connection with different deformation conditions. After Meyer and Robiller (133).

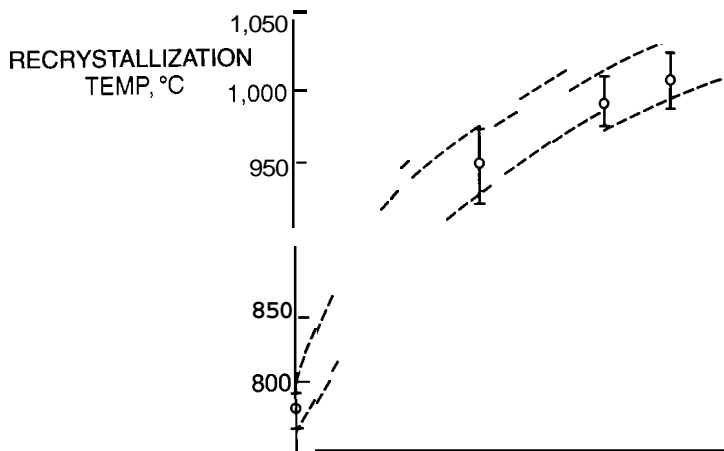


Figure 50 - The influence of niobium content on the recrystallization temperature of austenite as determined in hot compression testing. After Cuddy (139).

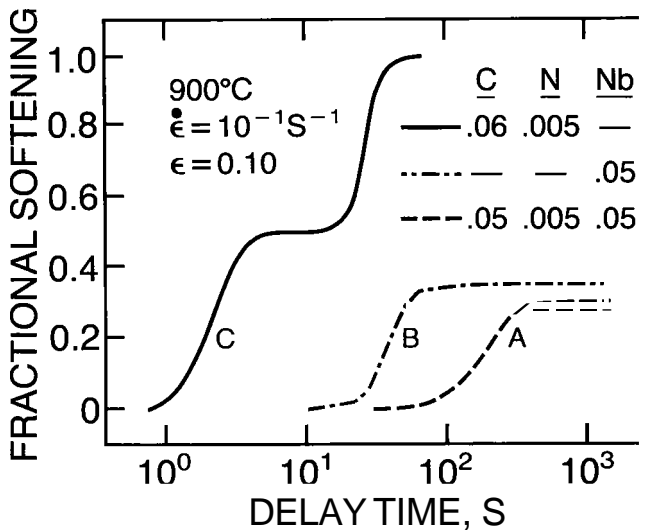


Figure 51 - Fractional softening versus delay time at 900 C. After Luton, et al (130).

where  $\sigma_1$  is the yield stress during the prestraining,  $\sigma_0$  is the flow stress just prior to unloading and  $\sigma_2$  is the proof stress on reloading. The static softening curves shown in Figure 51 exhibit either one or two sigmoidal portions. The first is interpreted to be static recovery and the second static recrystallization. The data shown in Figure 51 indicate that the base steel undergoes static recovery in about 5 seconds and static recrystallization within the next 10 seconds. The two Nb steels also undergo static recovery, although in much longer times. These steels, however, did not undergo static recrystallization during the  $10^3$  second holding time used in this experiment.

The precise manner in which Nb acts to retard static recrystallization has been a point of controversy for some time. The original hypothesis, based on electron metallography, was that Nb acted to suppress static recrystallization by precipitating on the cell walls of the unrecrystallized austenite, hence keeping the structure from being able to form viable nuclei for subsequent recrystallization, (95, 105, 116). The recent work of Jonas, et al., (114, 121) and Luton, (132) in addition to some earlier studies (112, 113) have suggested that it is, in fact, the Nb which is in solution which retards recrystallization and it does this by slowing down the rate of static recovery. It has been hypothesized that the retarding of recovery by Nb in solution permits the precipitation of NbCN to occur and further retard recrystallization. The implication is that if the recovery process were not retarded, the static recrystallization would occur before precipitation could take place.

If static recrystallization can be avoided during the holding times between rolling passes, for example, then the austenite will be able to store more energy in the form of crystalline defects such as excess grain boundary area per unit volume as well as a higher density of twins and deformation bands. A good example of this effect is taken from the work of Kozasu, et al., (16) and is shown in Figures 52 and 53. The increase in the effective austenite interfacial area per unit volume leads to a larger number of sites for ferrite nucleation during transformation, and, hence, to increased grain refinement. This grain refinement is shown in Figure 54.

To summarize then, Nb acts to raise the recrystallization temperature while also suppressing static recrystallization. This means that the addition of Nb to a C-Mn-Si steel will lead to at least four benefits:

For the same sequence of rolling reductions,

(A) More passes will occur below the recrystallization temperature, and the unrecrystallized austenite grains will be more highly elongated. This will act to increase the grain boundary surface area per unit volume and will lead to a larger number of sites per unit volume for ferrite nucleation.

(B) The small thickness of the elongated austenite grain will put an effective upper limit on the size of the resulting ferrite grains.

(C) The density of crystalline defects inside the elongated austenite grains will be higher and, hence, will lead to more sites for ferrite nucleation.

(D) Some of the austenite substructure will be transmitted into the ferrite and will lead to extra strengthening. With the portion of substructure retained tending to increase with a decrease in transformation temperature.

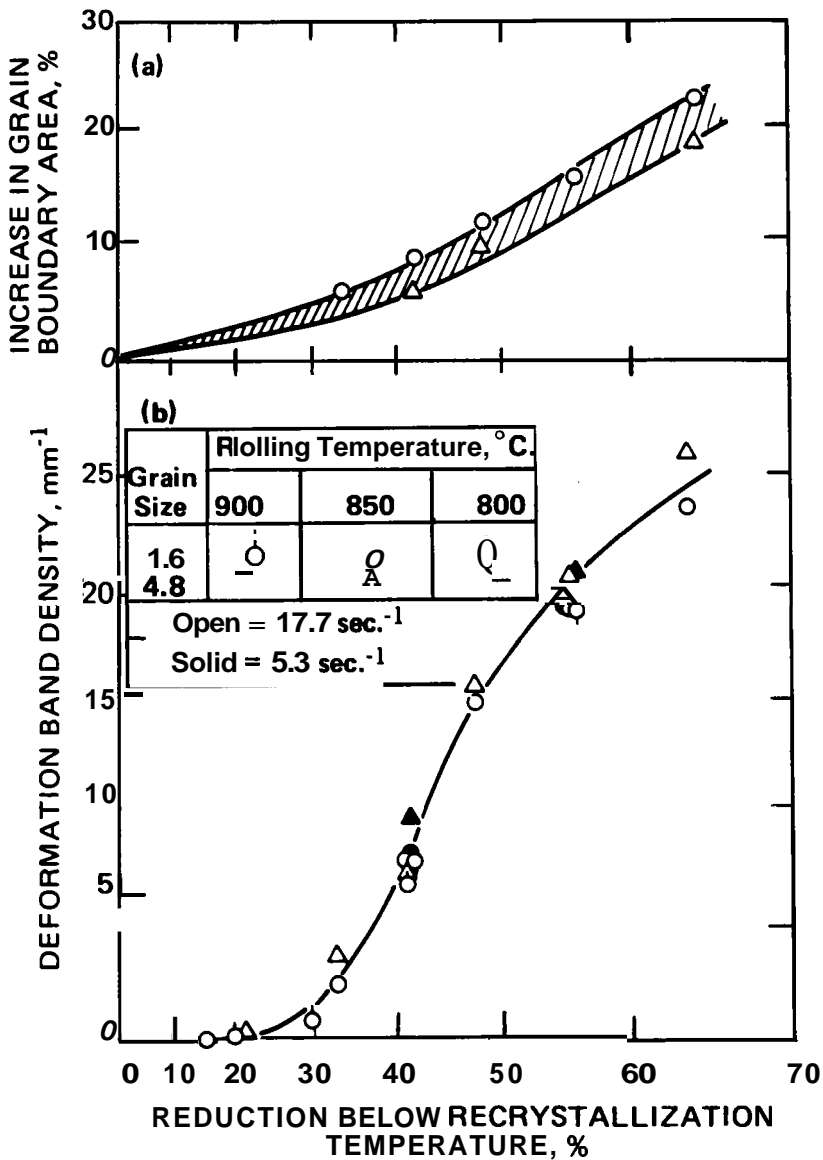


Figure 52 - Variation in austenite grain-boundary area and introduction of deformation bands resulting from rolling below the recrystallization temperature. In this 0.03 percent columbium steel, the initial grain size was varied by rolling in two passes at higher temperatures after reheating to 1250 C. After Kozasu et al (16).

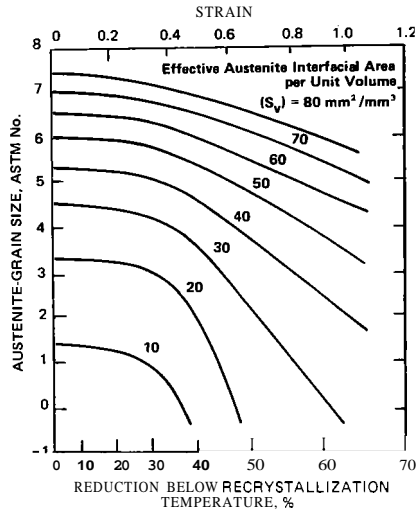


Figure 53 - Variation of effective interfacial area ( $S_v$ ) with rolling below the recrystallization temperature for the 0.03 percent columbian steel. After Kozasu et al (16).

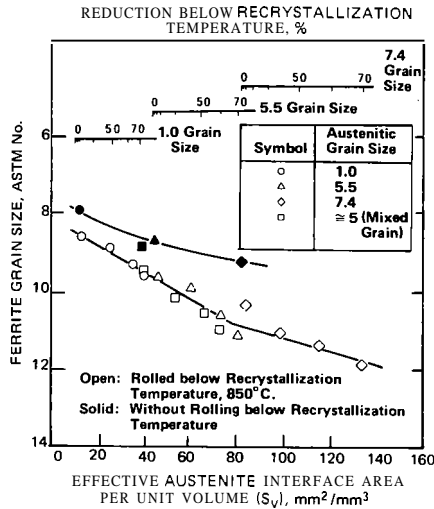


Figure 54 - Variation of ferrite-grain size with interfacial area ( $S_v$ ) in 0.03 percent columbian steel. After Kozasu et al (16).

Circumstantial evidence that niobium may lower polygonal ferrite start temperature was provided by Kazinczy, et al., (143) who observed the formation of widmansratten ferrite/bainite structures in hot-rolled plate steels with consequent disastrous effects on notch toughness. Later work by Ronn confirmed that the continuous cooling transformation behavior was substantially modified by niobium (144).

Niobium can increase the "hardenability" of austenite if it is in solid solution in a manner similar to boron, but can decrease the hardenability if it is out of solution as a result of austenite grain refinement. Furthermore, accumulation of strain (cold work) below the austenite recrystallization temperature (controlled by niobium content) will increase the  $\gamma + \alpha$  start temperature, Figure 55 (16). Thus, in practice the exact transformation conditions will depend on a balance between the competing factors of solution, reprecipitation, recovery and recrystallization and grain refinement.

Transformation diagrams for a plain carbon and a 0.11 percent niobium steel are shown in Figure 56 (145). The 0.11 percent Nb is essentially out of solution after being reheated at 900 C; this precipitation would result in grain refinement of the reheated structure, hence a lower hardenability than the base steel. However, after reheating at 1300 C, the 0.11 percent Nb is predominately in solution, and the resulting hardenability is much higher than in the base steel. Comparison of the effect of niobium with that of

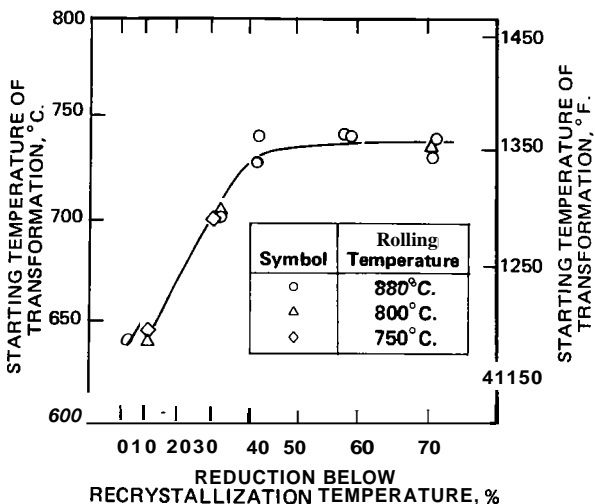


Figure 55 - Variation of the austenite-to-ferrite transformation temperature of 0.03 percent columbium steel with the deformation below the austenitic-recrystallization temperature. The steel was reheated to 1250 C, rolled at 850 C, and cooled at 25 C per second between 800 and 500 C. The  $A_r$  (900 C heating 25 C per second cooling) was 748 C. The initial grain size was 1.0. The transformation temperature was measured on a modified thermal analyzer. After Kozasu et al (16).

boron and molybdenum is shown in Figure 57. The rate of depression of the austenite ferrite start temperature is about equivalent to the effects found for optimum boron additions and is greater on a weight percent basis than traditional "hardenability" elements such as molybdenum.

The utility of using niobium to lower austenite-to-ferrite start temperature is limited due to its relatively low solubility. Thus, lower carbon contents and high reheating temperature will tend to maximize the effect, especially for unstrained austenite. The competition between the effects of solute niobium and austenite grain refinement are shown as a function of reheating temperature in Figure 58 (56). The change in austenite-to-ferrite start temperature is also austenite-grain-size dependent, Figure 59, (118) and reaches a maximum at large grain size.

Thus, in normal hot-rolling situations the effect of niobium in lowering the  $\gamma \rightarrow \alpha$  transformation temperature will be strongly countered by the reduction of niobium in solution as a result of strain-induced precipitation and by the "grain refinement" which results from the accumulated strain in the austenite (below the recrystallization temperature). This latter benefit is related to the effective interfacial area of the strained austenite, Figure 60 (16).

A crude quantitative measure of the effect of niobium on the  $\gamma \rightarrow \alpha$  start temperature can, when it is in solid solution, be obtained from the intersection of cooling curves with continuous cooling transformation diagrams for different steels. Available data from the literature are summarized in

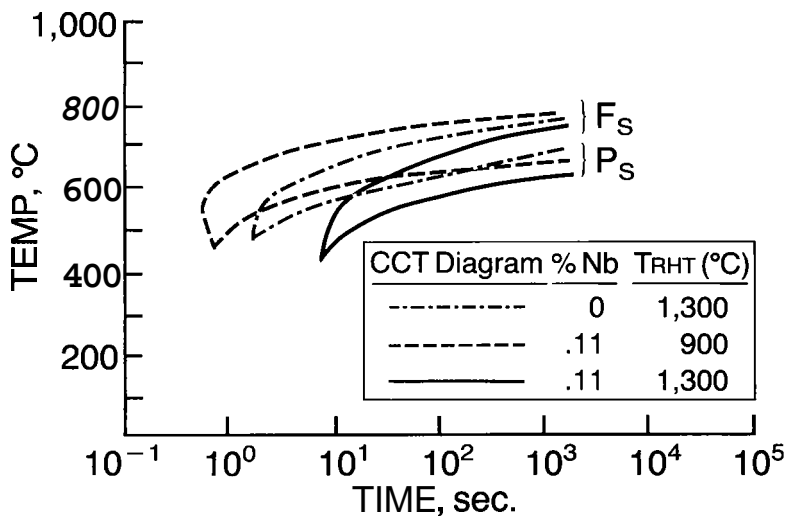


Figure 56 - Continuous-cooling-transformation diagram for three steels which contain 0.2 percent C and 1.2 percent Mn. After Meyer (145).

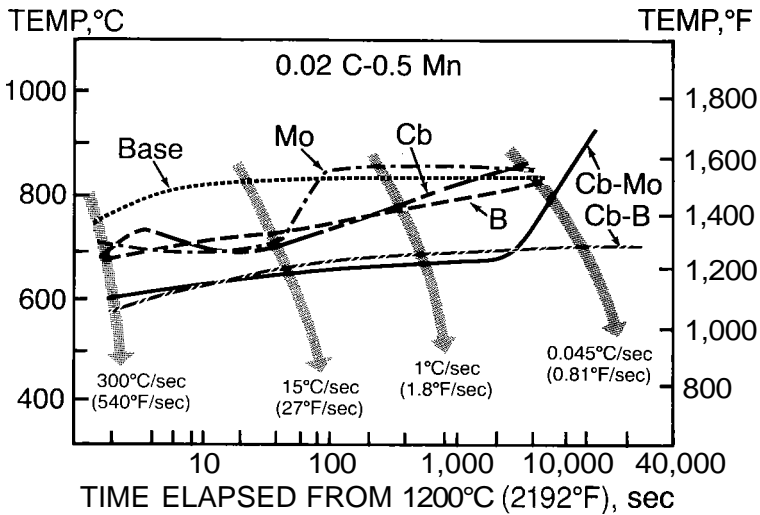


Figure 57 - A comparison of the effect of niobium with molybdenum and boron added singly or in combination on the ferrite start temperature. Undeformed austenite. After Gray (146).

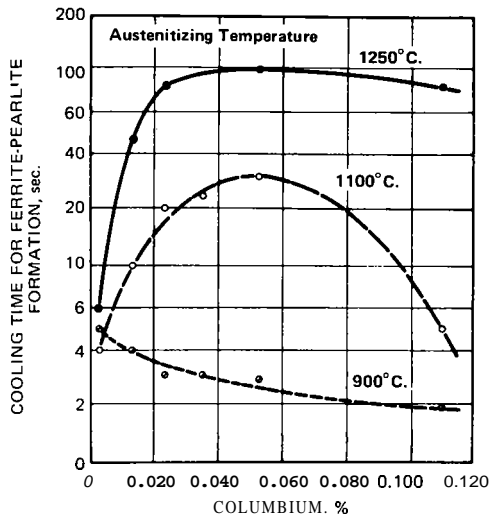


Figure 58 - Cooling time between 800 and 500 C for the start of ferrite-pearlite formation in columbium steels after austenitizing at different temperatures. The steel contained 0.2 percent carbon and 1.2 percent manganese. After Meyer, et al (56).

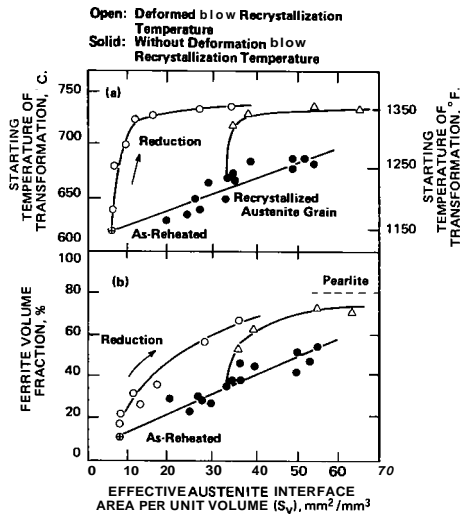
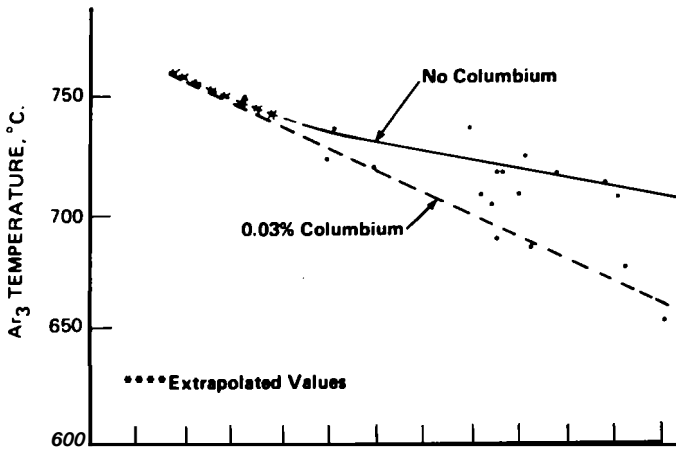


Figure 60 - Change of transformation behavior with variations in the effective interfacial area for 0.03 percent columbium steel reheated to 1250 C. The open circle shows the steels rolled by one pass at 880 C. The solid circle shows a fully recrystallized structure. After Kozasu et al (16).

Figure 61, (23, 147-151). For a cooling rate of  $5.5 \text{ C/sec}$ , 0.03 percent niobium lowers the ferrite start temperature by between 25 and 75 C. Note that the data of Cochrane and Kirkwood (23) and Harrison (149) are from weld metal where it is found that niobium modifies the as-cast microstructure (23). The effects of this on weld metal properties depend on the microstructure and transformation behavior in the absence of niobium.

### Reduction in Transformation

Start Temperature, °C

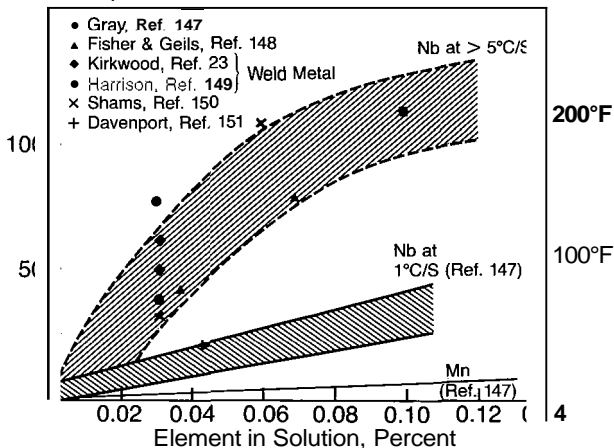


Figure 61 - The influence of niobium or manganese in solution on the lowering of the transformation start temperature.

It is interesting to note that on a weight percent basis, niobium is about 10 times more effective than manganese in lowering ferrite start temperature.

The importance of controlling the transformation temperature has been discussed by Gray (152) and Wilson and Gray; (153) these studies have shown that low transformation temperatures promote finer ferrite grains, larger increments of precipitation hardening and higher yield strengths. Figure 62 shows these relationships.

There are several ways of obtaining low transformation temperatures. One way is to maximize soluble Nb contents by using low carbon contents and high reheating temperatures; this would ensure that a large amount of Nb would be taken into solution during reheating. A portion of the Nb would be precipitated as strain-induced NbCN during hot rolling, but much of the Nb would still be supersaturated in the austenite and could act to lower the transformation temperature. Other elements, such as Cr, Mo, Mn and Ni, can also lower the transformation temperature, (154) as illustrated in Figure 63 for different ratios of Mn and Ni.

Practical use of these "hardenability" effects have been made in producing several low-carbon bainitic steels (155-157).

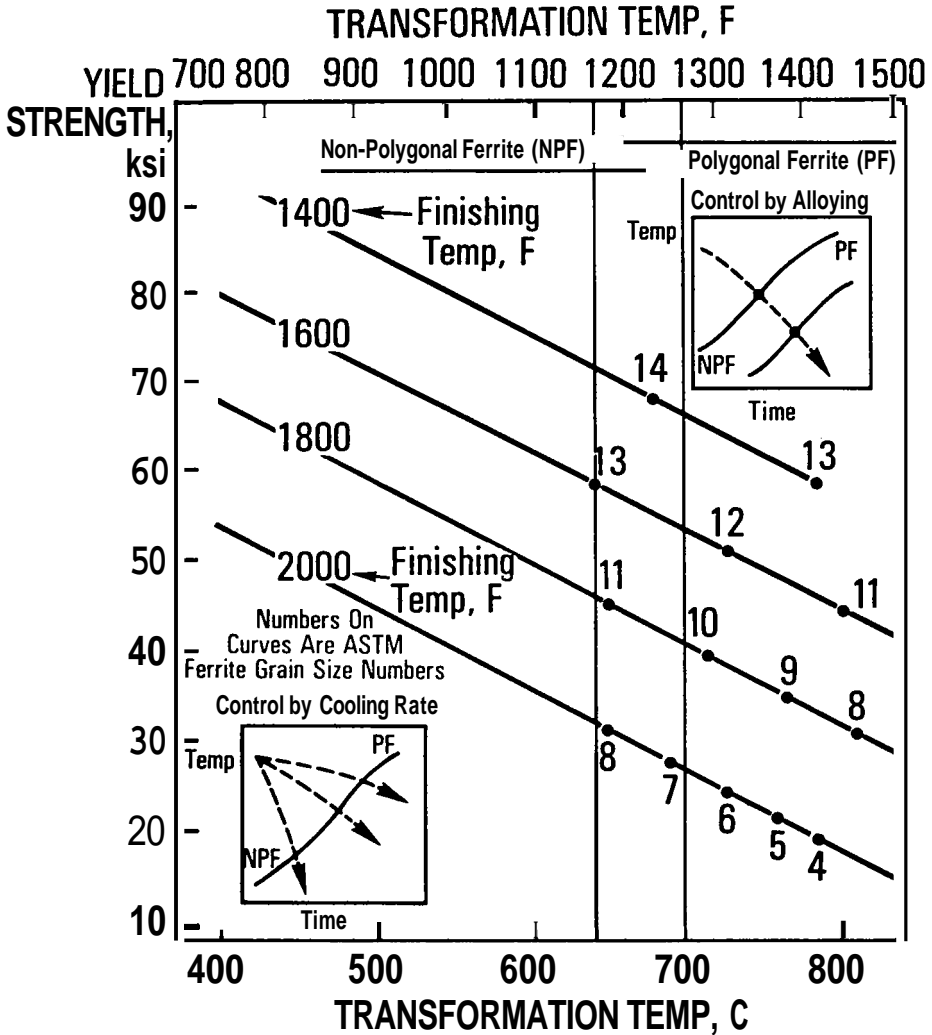


Figure 62 - The effect of transformation temperature on the yield strength of a niobium-bearing HSLA steel. After Gray (152).

Substructure and Texture Effects

Recent trends toward lower finish rolling and transformation temperatures have resulted in an increased awareness of the importance of substructural and textural strengthening in hot-rolled steels (34). The magnitudes of these strengthening mechanisms relative to others is shown in Figure 64.

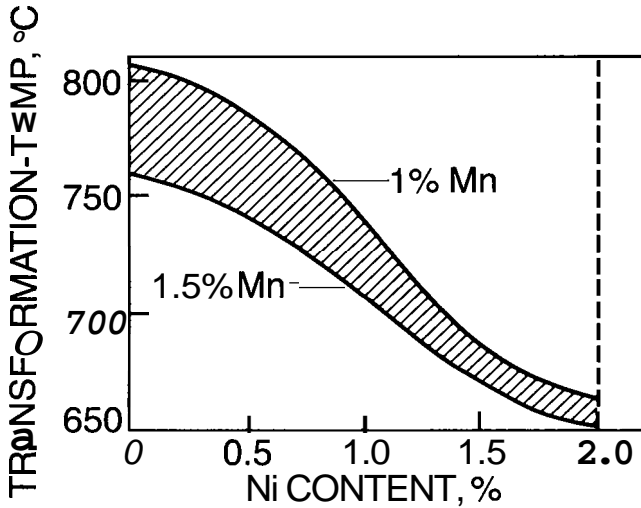


Figure 63 - Relationship between transformation temperature, nickel and manganese - content in low carbon niobium steels. After Heisterkamp et al (154).

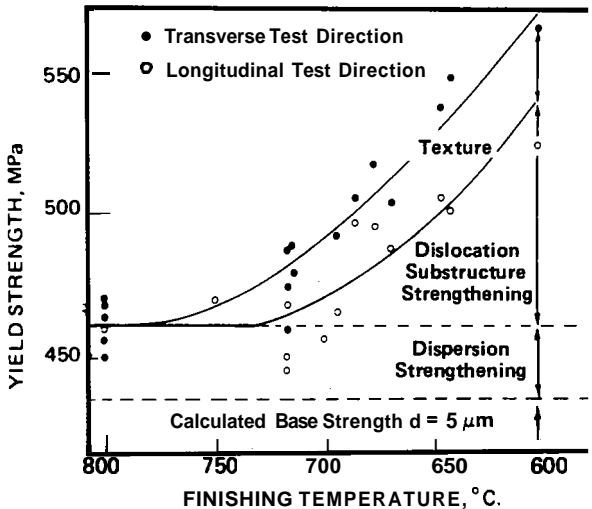


Figure 64 - Analysis of factors contributing to the strength of low-temperature rolled HSLA plate. After Gladman et al (34).

## Summary

The last quarter century has witnessed the evolution of microalloyed HSLA steels, especially niobium-bearing steels, from being laboratory curiosities to being economically viable engineering materials. These steels provide excellent mechanical properties at a low cost, and are, therefore, attractive structural materials for the energy, transportation and construction industries. An additional benefit of these steels is that they can nearly always be used in the as-processed condition. This eliminates the need for subsequent heat treatments; hence, these steels are relatively energy non-intensive.

The attractive mechanical properties exhibited by these steels result from the control of metallurgical microstructure. Research over the last two decades has illustrated that the properties, i.e. microstructure, of the steel result from a complex interaction between steel composition and processing. The purpose of this paper has been to review some of the research that has been conducted concerning the relationships that exist among composition, processing and properties of these steels. Work of this type permits a better understanding of contemporary HSLA steels and, at the same time, shows the way to more improved steels in the future.

## References

1. W. B. Morrison and J. H. Woodhead, J. Iron and Steel Inst., 1963, V. 201, 43.
2. K. J. Irvine and F. B. Pickering, Ibid., 944.
3. T. M. Noren-Brandel, "Columbium as a Micro-Alloying Element in Steels and its Effect on Welding Technology", SSC-154 Special Report US Department of Commerce, Office of Technical Services PB181539, August 30, 1963.
4. F. deKazinczy, A. Axnas and P. Pachleitner, Jernkont. Ann., 1963, V. 147, 408.
5. Metallurgical Developments in Carbon Steels, I.S.I. Special Report No. 81, The Iron and Steel Institute, London, 1963.
6. Symposium on Low-Alloy High-Strength Steels, The Metallurg Companies, Nuremberg, BRD, 1970.
7. Processing and Properties of Low Carbon Steels, J. M. Gray, Editor, AIME, New York, 1973.
8. Microalloying 75, M. Korchynsky, et al., Editors, Union Carbide Corporation, New York, 1977.
9. The Hot Deformation of Austenite, J. Ballance, Editor, TMS-AIME, New York, 1976.
10. Recrystallization in the Development of Microstructure (Leeds), Met. Sci., 1979. V. 13.
11. Hot Working and Forming Processes (Sheffield), C. M. Sellars and G. J. Davies, Editors, The Met. Soc., London, 1980.

12. RISO International Symposium on Recrystallization and Grain Growth of Multi-Phase and Particle-Containing Materials, Hansen, Jones and Leffers, Editors, RISO National Laboratory, Denmark, 1980.
13. International Conference on Steel Rolling, The Iron and Steel Inst. of Japan, Tokyo, 1980.
14. A. B. Lebon and L. N. deSaint-Martin, Reference 8, p. 90.
15. P. Mangonon and W. E. Heitmann, Reference 8, p. 59.
16. I. Kozasu, C. Ouchi, T. Sampei and T. Okita, Reference 8, p. 120.
17. P. Wellner, A. Mukherjee and H. Meyer, Sulzer Technical Review, Winterthur, Switzerland, Feb. 1976, 69.
18. P. Wellner and B. Walser, Metal Progress, 1981, V. 119, NO. 6, p. 45.
19. Wallace, Ti Grain Refinement, Ref. 7.
20. V. K. Heikkinen and R. H. Packwood, Scand. J. Metallurgy, 1977, V. 6, 170.
21. G. Bernard, Reference 8, p. 552.
22. R. Jesseman, Reference 8, p. 578.
23. P. R. Kirkwood, This conference.
24. J. N. Cordea, Reference 6, p. 61.
25. J. M. Chilton and M. J. Roberts, Vanadium in High-Strength Steel (Chicago), Vanitec, London, 1980, 11.
26. M. L. Santella and A. J. DeArdo, Thermomechanical Processing of Microalloyed Austenite, A. J. DeArdo, Editor, AIME, Warrendale, Pa., 1982, In Press.
27. L. J. Cuddy, J. J. Bauwin and J. C. Raley, Metall. Trans., 1980, V. 11A, 381.
28. T. Tanaka, N. Tabata, T. Hatomura and C. Shiga, Reference 8, p. 107.
29. C. Ouchi, T. Sampei, T. Okita and I. Kozasu, Reference 9, p. 316.
30. D. B. McCutcheon, Paper presented at Journ e Internationale de Siderurgie, Paris, France, October 4, 1974.
31. H. Ohtani, T. Hashimoto and Y. Fujishiro, Lecture S557, 101st ISIJ Meeting, April 1981, Tokyo, Japan.
32. H. Sekine and T. Maruyama, Microstructure and Design of Alloys, Iron and Steel Society, ISI Report No. 36, London, 1973.
33. R. Coladas, J. Masounave and J. P. Bailon, Reference 9, p. 378.
34. T. Gladman, D. Dulleu and I. D. McIvor, Reference 8, p. 32.

35. R. Shaughnesy, et al., "Method of Producing Steel Which Has High Strength and High Notch Impact Toughness", German Patent No. 2323738, May 10, 1973.
36. W. E. Heitmann, et al., The 13th Annual CIM Conference of Metallurgists, Toronto, August 25-28, 1974.
37. U. Lotter and L. Meyer, Metals Technology, January 1977, p. 27.
38. T. Irie, et al., Kawasaki Technical Report #2, March 1981, p. 14.
39. P. R. Mould and J. M. Gray, Metall. Trans., 1972, Vol. 3, 3121.
40. J. M. Gray and R. B. G. Yeo, Transactions Quarterly AIME, Vol. 61, 1968.
41. P. R. Hastings and N. Couture, CIM Conference of Metallurgists, Vancouver, B. C., August 21-25, 1977.
42. D. Webster, Ph.D. Thesis, University of Sheffield, 1965; also D. Webster and J. H. Woodhead, J. Iron Steel Inst., 1969, V. 202, 987.
43. J. H. Woodhead, Reference 25, p. 1.
44. H. Gondoh and T. Osuka, This conference.
45. H. Baumgardt, H. deBoer, F. Heisterkamp, This conference.
46. H. Takechi, et al., Ref. 8, p. 957.
47. W. F. Smith, Structure and Properties of Engineering Alloys, 1981, McGraw-Hill, New York.
48. R. P. Elliot, Constitution of Binary Alloys, First Supplement, 1965, McGraw-Hill, New York, 155.
49. Y. Adda and J. Philibert, La Diffusion Dans Les Solides, Institut National Des Sciences et Techniques Nucleaires, Sunday, 1966.
50. G. M. Leak, Communication with J. Barford, J. Iron Steel Inst., 1966, V. 204, 134.
51. R. Summerling and J. Nutting, J. Iron Steel Inst., 1965, V. 203, 398.
52. Y. Imai and J. Masumoto, Tetsu to Hagane, 1961, v. 47, 139.
53. S. Kurokawa, et al., 36th ABM Annual Congress, 5-10 July 1981, Recife, Brasil.
54. K. Narita, Trans. Iron Steel Inst., Japan, 1975, V. 15, 145.
55. A. McLean and D. A. R. Kay, Reference 8, p. 215.
56. L. Meyer, F. Heisterkamp and W. Mueschenborn, Reference 8, p. 153.
57. G. Bauer, H. Renner and J. Wernet, Z. anorg. allgem. Chem., 1954, V. 277, 249.

58. G. Bauer and R. Lesser, Z. Metallk., 1959, V. 50, 8.
59. E. K. Storms and N. H. Krikorian, J. Phys. Chem., 1960, V. 64, 1747.
60. M. L. Pochon, et al., Reactive Metals, Vol. 2, Interscience, New York, 1959, 327.
61. R. P. Elliot, Armour Research Foundation Report, ARF-2120-4, 1959.
62. E. K. Storms and N. H. Krikorian, J. Phys. Chem., 1960, Vol. 64, 1471.
63. P. Schwaab, G. Langenscheid, Prakt Metallogr., 1972, No. 2, p. 67.
64. C. J. Smithells, Metals Reference Book, 4th Ed., 1967, Butterworths, London, 155.
65. H. Wantanabe, Y. E. Smith and R. D. Pehlke, Reference 9, p. 140.
66. T. Mori, et al., Tetsu-to-Hagane, 1964, V. 50, 911.
67. W. A. Randi, United States Steel Corporation Research Laboratories, Pittsburgh, Pa., 1979, Private Communication.
68. L. Meyer, H. Buhler and F. Heisterkamp, Thyssen Forschung, 1971, August Thyssen-Hütte AG, Duisburg-Hamborn, 8.
69. M. L. Santella, University of Pittsburgh, Department of Metallurgical and Materials Engineering, Ph.D. Thesis, 1981.
70. W. B. Pearson, Handbook of Lattice Spacings and Structures of Metals and Alloys, V. 2, 1967, Pergamon Press.
71. P. Duwez and F. Odell, J. Electrochem., 1950, V. 97, 299.
72. G. Brauer and R. Lesser, Z. F. Metallk., 1959, V. 50, 487.
73. J. M. Gray, Proceedings: "Heat Treatment 73", Metal Society, London, 1973.
74. G. Brauer and J. Jander, Z. anorg. Chem., 1952, V. 270, 160.
75. R. P. Elliott, Trans. ASM, 1961, V. 53, 31.
76. S. Kanazawa, et al., J. Japan Inst. Metals, 1967, V. 31, 171.
77. G. Krapf, et al., J. Iron Steel Inst., 1973, V. 221, 353.
78. H. Nordberg and B. Aronson, J. Iron Steel Inst., 1968, V. 206, 1263.
79. P. Mandry and W. Dornelas, Compt. Rend., 1966, V. 263, 1118.
80. C. Ouchi, To appear in Trans. Iron Steel Inst. Japan, 1981.
81. A. Grimaldi, et al., Arch Eisenhüttenwesen, 1967, V. 38, 401.
82. T. Mori, et al., Tetsu-to-Hagane, 1965, V. 51, 2031.
83. S. Maneschi and AM. Beccaria, Met. Ital., 1966, V. 1, 19.

84. Hoesch-Estel, Dortmund, Unpublished results.
85. W. A. Roberts, A. Sandberg and T. Siwecki, Vanadium Steels (Krakow), VANITEC, London, 1981, 19.
86. E. L. Brown, A. J. DeArdo and J. H. Bucher, Reference 9, p. 250.
87. R. E. Reed-Hill, Physical Metallurgy Principles, Second Ed., 1973, Van Nostrand, New York, 661.
88. R. E. Reed-Hill, Reference 87, p. 480.
89. F. E. Listhuber, Reference 6, p. 29.
90. J. Wadsworth, J. H. Woodhead and S. R. Keown, Met. Sci., 1976, V. 10, 362.
91. S. R. Keown and W. G. Wilson, Reference 26, In press.
92. S. Koyama, T. Ishii and K. Narita, Kinzoku Gakkai-shi, 1971, V. 35 No. 11, 1089.
93. R. Simoneau, G. Begin and A. H. Marquis, Met. Sci., 1978, V. 12, 381.
94. D. H. Jack and K. H. Jack, Mats. Sci. and Eng., 1973, V. 11, 1.
95. A. T. Davenport, L. C. Brossard and R. E. Miner, J. Metals, 1975, V. 27, 21.
96. R. W. K. Honeycombe, Metall. Trans., 1976, V. 7A, 915.
97. J. M. Silcock, J. Iron Steel Inst., 1963, V. 201, 409.
98. J. S. T. Van Aswegen, R. W. K. Honeycombe and D. H. Warrington, Acta Met., 1964, V. 12, 1.
99. J. M. Silcock, Acta Met., 1966, V. 14, 687.
100. F. H. Froes, R. W. K. Honeycombe and D. H. Warrington, Acta Met., 1967, V. 15, 157.
101. M. Tanino and K. Aoki, Trans. Iron Steel Inst. Japan, 1968, V. 8, 337.
102. R. G. Baker and J. Nutting, Precipitation Processes in Steels, ISI Spec. Report No. 64, London, 1959, 1.
103. G. Kurdjumov and G. Sachs, Zeit. f. Physik, 1930, V. 62, 592.
104. G. Gauthier and A. S. LeBon, Reference 3, p. 71.
105. A. T. Davenport, R. E. Miner and R. A. Kot, Reference 9, p. 186.
106. J. Irvine and T. N. Baker, Met. Sci., 1979, V. 13, 228.
107. S. S. Hansen, J. S. Vander Sande and M. Cohen, Metall. Trans., 1980, V. 11A, 387.
108. A. Mascanzoni and G. Bussichelli, Phil. Mag., 1974, V. 30, 207.

109. S. Freeman, Effect of Second Phase Particles on the Mechanical Properties of Steel, ISI Special Publication No. 145, London, 1971, 152.
110. E. Orowan, Symposium on Internal Stresses, Inst. of Metals, London, 1947, 451.
111. M. F. Ashby, Proc. Second Bolton Landing Conference on Oxide Dispersion Strengthening, Gordon and Breach, New York, 1968.
112. A. LeBon, J. Rofes-Vernis and C. Rossard, Metals Sci., 1975, V. 9, 36.
113. R. Colada, J. Masounave and J. P. Bailon, Reference 9, p. 378.
114. J. J. Jonas and I. Weiss, Metals Sci., 1979, V. 13, 238.
115. D. Webster and J. A. Woohed, J. Iron Steel Inst., 1964, V. 202, 987.
116. J. D. Jones and A. R. Rothwell, Deformation Under Hot Working Conditions, 1968, ISI Publication No. 108, London, 78.
117. J. M. Gray, Reference 7, p. 225.
118. T. M. Hoogendorn and M. H. Spanraft, Reference 8, p. 75.
119. G. Bégín and R. Simoneau, Reference 8, p. 85.
120. R. K. Amin, G. Sutterworth and F. B. Pickering, Reference 11, p. 27.
121. M. G. Akben, I. Weiss and J. J. Jonas, Acta Met., 1981, V. 29, 111.
122. C. S. Smith, Trans. AIME, 1948, V. 175, 15.
123. I. Weiss, G. Fitzsimons, K. Tiitto and A. J. DeArdo, Reference 26, In press.
124. P. Feltham, Acta Met., 1957, V. 5, 97.
125. J. D. Verhoeven, Fundamentals of Physical Metallurgy, 1975, Wiley, New York, 201.
126. R. E. Reed-Hill, Reference 87, p. 298.
127. J. D. Verhoeven, Reference 125, p. 354.
128. R. E. Reed-Hill, Reference 87, p. 318.
129. T. Gladman and F. B. Pickering, J. Iron Steel Inst., 1967, V. 205, 653.
130. R. A. Petkovic, M. J. Luton and J. J. Jonas, Reference 9, p. 68.
131. M. J. Stewart, Reference 9, p. 233.
132. M. J. Luton, R. Dorvel and R. A. Petkovic, Metall. Trans., 1980, V. 11A, 411.
133. L. Meyer and G. Robiller, Reference 12, p. 311.

134. I. Weiss, G. Fitzsimons, K. Tiitto, and A. J. DeArdo, Reference 26, In press.
135. J. J. Jonas, C. M. Sellars and W. J. McG. Tegart, Metall. Rev., 1969, V. 14, 1.
136. H. J. McQueen and J. J. Jonas, Plastic Deformation of Materials, R. J. Arsenault, Editor, 1975, Academic Press, New York, 393.
137. K. J. Irvine, T. Gladman, J. Orr and F. S. Pickering, J. Iron Steel Inst., 1970, V. 208, 717.
138. T. G. Oakwood, W. E. Heitmann and E. S. Madrzyk, Reference 9, p. 204.
139. L. J. Cuddy, United States Steel Corporation Research Laboratory, Pittsburgh, Pennsylvania, 1981, Private communication.
140. M. Korchynsky and H. Stuart, Reference 6, p. 17.
141. T. Greday and M. Lamberigts, Reference 8, p. 172.
142. W. J. McG. Tegart, Reference 9, p. 1.
143. F. deKazinczy, A. Axnas, and P. Pachleitner, Jernkont Ann, 1963, V. 147, 408.
144. L. Ronn, "Niobs inverkan pa TTT-diagrammet av ett mjukt stal", Thesis for the degree of metallurgical engineer, The Royal Institute of Technology, Stockholm, Sweden, 1963.
145. L. Meyer, Thyssen Aktiengesellschaft, Duisburg-Hamborn, 1981, Private communication.
146. J. M. Gray, 'Weldability of Niobium-Containing High-Strength Low-Alloy Steel', Welding Research Council Bulletin No. 213, February 1976.
147. J. M. Gray, Heat Treatment '73, The Metals Society London, 1974, 19.
148. G. L. Fisher and R. H. Geils, presented at the TMS-AIME Fall Meeting, Detroit, October 1968 (Unpublished).
149. P. L. Harrison, et al., Welding and Metal Fabrication, April 1981, 161.
150. N. Shams, Yearly Report, Department of Metallurgy, University of Sheffield, 1980.
151. A. T. Davenport, Republic Steel Corporation Research Laboratory, Independence Ohio, 1981, Private communication.
152. J. M. Gray, Metall. Trans., 1972, V. 3, 1495.
153. J. M. Gray and W. G. Wilson, 14th Mechanical Working and Steel Processing Conference, 1972, AIME, New York.
154. F. Heisterkamp, J. M. Gray and H. Stuart, Second International Conference on Pipewelding, 1979, London, 307.

155. H. Matsuda, et al., "Development of Controlled-Rolled Bainitic Steel for Large Diameter Linepipe", Preprint, Conference on Alloys for the 80's, Climax Molybdenum Co., Ann Arbor, Michigan, June 17-18, 1980.
156. A. Massip and L. Meyer, Stahl u Eisen, 98, 1978, N° 19, p. 989.
157. B. Serin, et al., Mem. Sci. Rev. Met., 1978, p. 355.